

Differentiating and Integrating ZX Diagrams with Applications to Quantum Machine Learning

Quanlong Wang^{*1}, Richie Yeung^{*2,1}, and Mark Koch^{*3}

¹Quantinuum, 17 Beaumont Street, Oxford, OX1 2NA, United Kingdom

²University of Oxford, United Kingdom

³Quantinuum, Terrington House, 13-15 Hills Road, CB2 1NL Cambridge, United Kingdom

ZX-calculus has proved to be a useful tool for quantum technology with a wide range of successful applications. Most of these applications are of an algebraic nature. However, other tasks that involve differentiation and integration remain unreachable with current ZX techniques. Here we elevate ZX to an analytical perspective by realising differentiation and integration entirely within the framework of ZX-calculus. We explicitly illustrate the new analytic framework of ZX-calculus by applying it in context of quantum machine learning for the analysis of barren plateaus.

1 Introduction

ZX-calculus is a powerful graphical rewrite system proposed by Coecke and Duncan [11] for linear maps, particularly for quantum circuits. A node with n edges in a ZX diagram, like in tensor network notation, represents an order n tensor. Moreover, it is possible to directly evaluate the tensor by performing local rewrites (i.e., substitution of a part of a ZX diagram). Using these local rewrites, ZX-calculus has been successfully applied to circuit compilation [4, 5, 18, 43], measurement-based quantum computing [27, 19], fusion-based quantum computing [8], quantum error correction [26, 6], quantum natural language processing [14, 34, 25], and quantum foundations [2, 13, 12, 20]. ZX-calculus can even be used as a concrete realisation of quantum theory [15]. These applications of ZX-calculus are algebraic in nature, and take advantage of *rewriting as a form of computation*: in fact ZX-calculus is a sound, universal [10] and complete [23] proof system that serves as an alternative to traditional linear algebra, which also makes it a different formalism from tensor networks. However, without the analytical tools of differentiation and integration, ZX-calculus fell short of tackling variational problems such as quantum machine learning or realising a comprehensive version of quantum mechanics including quantum dynamics.

In this paper we give for the first time rules for differentiating arbitrary ZX diagrams and integrating a wide class of ZX diagrams (including quantum circuits), within the framework of a slightly extended version of ZX-calculus called algebraic ZX-calculus [47] which makes it very convenient to deal with sums of ZX diagrams, thus paving the way for an analytical version of ZX-calculus. We apply these new techniques to develop a framework for a purely ZX-based analysis of the barren plateau phenomenon from quantum machine learning.

Quanlong Wang*: harny.wang@quantinuum.com

Richie Yeung*: richie.yeung@quantinuum.com

Mark Koch*: mark.koch@quantinuum.com

*Equal contribution

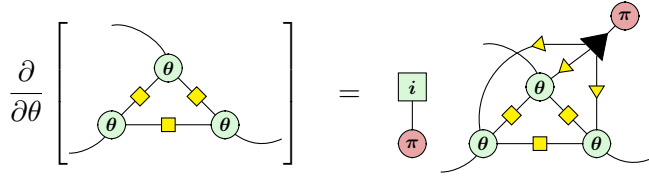


Figure 1: Example of diagrammatic differentiation.

Related Work

There have been previous attempts at providing rules for differentiating and integrating ZX diagrams [51, 45, 52]. In particular, Zhao and Gao [52] pioneered the use of ZX-calculus to aid in the analysis of the barren plateau phenomenon. Similar techniques were also used in [36] to study quantum tensor network ansätze. However, by explicitly using Hilbert space operations such as addition, all these previous attempts fall outside the realm of vanilla ZX-calculus as there are few techniques to further manipulate sums of diagrams. Ultimately, all previous works studying barren plateaus in the ZX-calculus had to resort to a combination of ZX diagrams and general tensor networks in order to handle this summation problem. The analytical ZX techniques developed in this paper on the other hand offer a unified framework to reason about differentiation and integration purely in terms of rewriting, without having to fall back to arbitrary tensor networks.

Previous attempts to formalise sums of ZX diagrams include work by Stollenwerk and Hadfield [44] who provide notation for representing sums of ZX diagrams as a single diagram by extending the ZX calculus with a pair of sum boxes which were later formalised by Villoria, Batsold, and Laarman [46]. However, this approach does not offer much additional diagrammatic reasoning power since it is merely syntactic sugar for writing linear combinations of diagrams. Jeandel, Perdrix, and Veshchezerova [24] independently derived an alternate method to represent sums and derivatives with the ZX-calculus by showing how the sum of two controlled ZX diagrams can be represented as a single controlled ZX diagram. However, their approach requires an inductive translation of diagrams to controlled diagrams such that the result will not resemble the original diagram. Our method on the other hand preserves diagram structure and can be calculated almost instantly. We refer to Appendix D for a more thorough comparison of the two approaches.

Finally, our approach also offers a numerical advantage: The tensor networks considered in [52, 36] have bond dimension 3 whereas all our diagrams only have dimension 2, yielding a speed-up when contracting the diagram in software. This was exploited in [31] to numerically detect the presence of barren plateaus by contracting diagrams representing the gradient variance of ansätze and observing the decay. Crucially, that work builds on our diagrammatic barren plateau framework developed in this paper, making use of the more efficient 2-dimensional representation compared to [52, 36]. Furthermore, the techniques developed in our work have QML applications beyond barren plateaus. For example, our results have been used in [30] to analyse and derive novel parameter shift rules for gradient computation using ZX.

Summary of results

1. Differentiation of arbitrary (algebraic) ZX diagrams, with a unified diagrammatic chain and product rule. (Theorem 14 and Theorem 16)
2. Definite integration of circuit-like ZX diagrams, with up to 3 occurrences of a parameter. (Proposition 32, Theorem 33, and Theorem 34)

3. Diagrammatic formula for the expectation and variance of a quantum circuit's gradient $\frac{\partial \langle H \rangle}{\partial \theta_i}$. (Lemma 35 and Theorem 38)
4. Demonstration of barren plateau analysis for an example ansatz. (Section 5.2)

From a general ZX-calculus perspective, this is the first paper to combine sums of ZX diagrams into a single ZX diagram in a methodical way. In particular, we highlight the importance of the W spider in ZX-calculus, which corresponds to the derivation structure of the product rule. These results required the combined power of the Z, X and W spiders, all 3 of which can be naturally represented within algebraic ZX-calculus.

Note: For presentation purposes, the proofs of some theorems and lemmas are moved to the appendix.

2 Algebraic ZX-calculus

The generators of the original ZX-calculus [11] are chosen with the aim to conveniently represent quantum computational models using complementary observables. On the other hand, the ZW-calculus [22] is designed based on the GHZ and W states, two maximally entangled quantum states [16]. It is known that the Z and W spiders from ZW-calculus act as the multiplication and addition monoid respectively, making it possible to perform arithmetic [17, 22].



We will see that the W state is crucial for dealing with sums of diagrams, and it is in fact closely related to the product rule used in differentiation. Conveniently, algebraic ZX-calculus [47] compactly decomposes the W spider and other gadgets such as the logical AND gate [38], into Z spiders, X spiders and triangle gates, thus giving us the benefits of ZX and ZW calculus within a single unified framework.



The yellow triangle of algebraic ZX-calculus is powerful as it sends the computational basis to a non-orthogonal basis, which makes diagrammatic representation and calculation of other logical gates much simpler. Conversely, the representation of the yellow triangle using other graphical calculi is more complicated. Intuitively, this is because the triangle gate is a low-level primitive in comparison to the Z, X, W and H spiders [3]. This algebraic extension of ZX is a universal and complete language for not just complex numbers, but also commutative rings and semirings [49].

In this section, we give an introduction to the algebraic ZX-calculus, including its generators and rewriting rules. In this paper ZX diagrams are either read from left to right or top to bottom.

2.1 Generators

The diagrams in algebraic ZX-calculus are defined by freely combining the following generating objects:

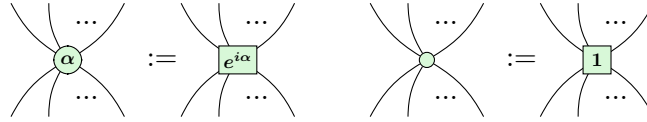
$R_{Z,a}^{(n,m)} : n \rightarrow m$		$\mathbb{I} : 1 \rightarrow 1$	
$H : 1 \rightarrow 1$		$\sigma : 2 \rightarrow 2$	
$C_a : 0 \rightarrow 2$		$C_u : 2 \rightarrow 0$	
$T : 1 \rightarrow 1$		$T^{-1} : 1 \rightarrow 1$	

Table 1: Generators of algebraic ZX-calculus, where $m, n \in \mathbb{N}$, $a \in \mathbb{C}$.

2.2 Additional notation

For simplicity, we introduce additional notation based on the given generators:

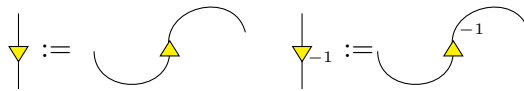
1. The green spider from the original ZX-calculus can be defined using the green box spider in algebraic ZX-calculus.



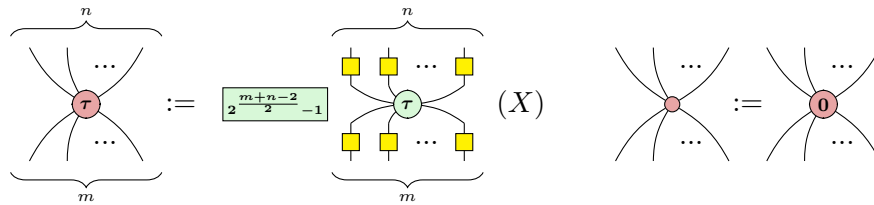
2. The whitespace around a diagram can be interpreted as an explicit horizontal composition with the empty diagram.



3. The transposes of the triangle and the inverse triangle can be drawn as an inverted triangle.



4. The pink spider is the algebraic equivalent of the red spider from the original ZX-calculus. It is only defined for $\tau \in \{0, \pi\}$, and is rescaled to have integer components in its matrix representation.

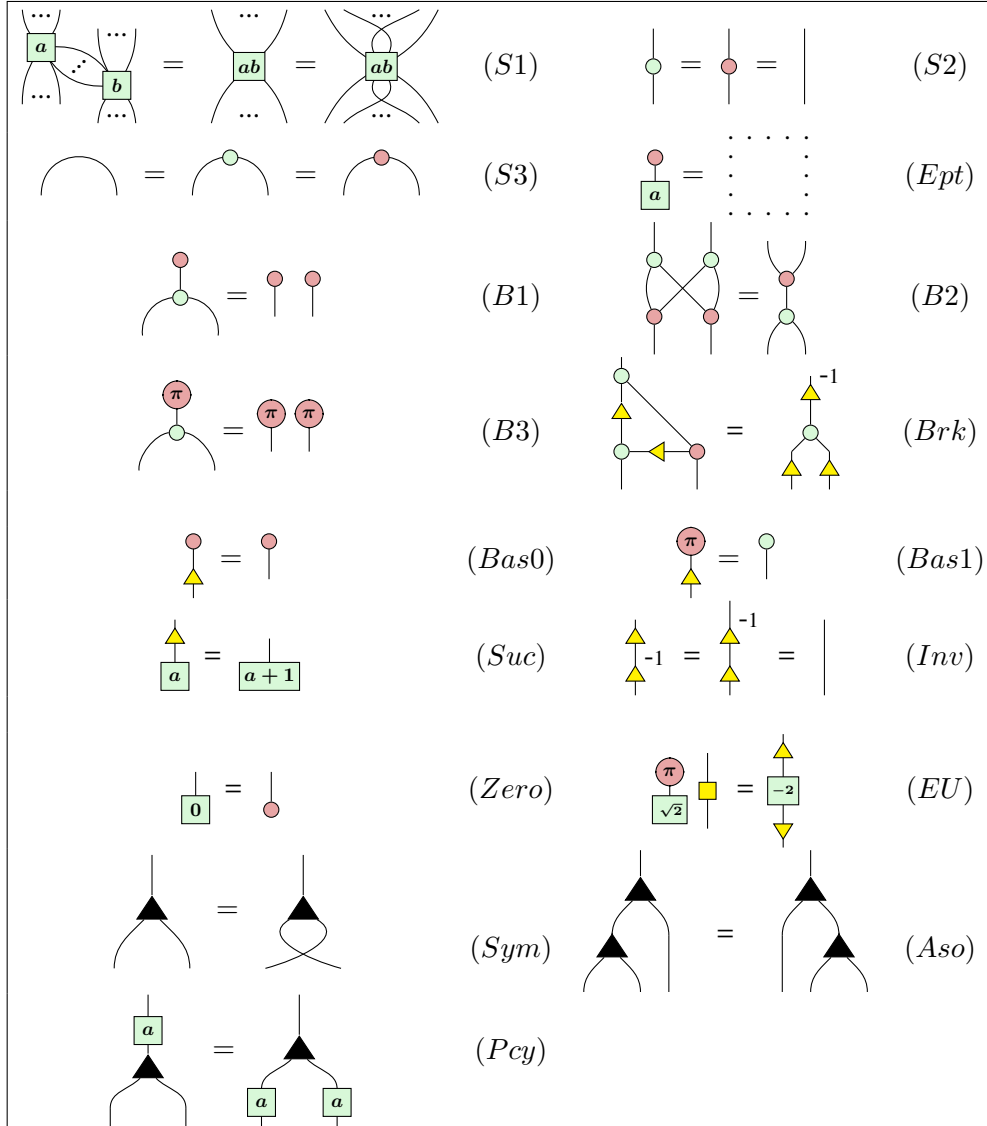


Note that the green box represents the scalar $\frac{2^{m+n-2}}{2} - 1 = 2^{\frac{m+n-2}{2}}$.

5. The W spider from ZW-calculus can be expressed as follows.

2.4 Rules

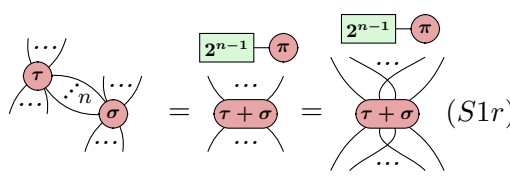
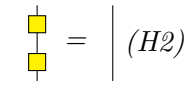
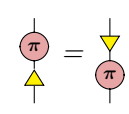
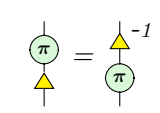
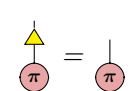
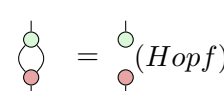
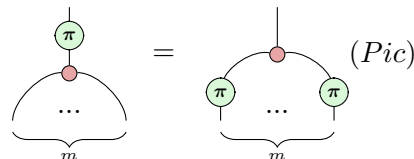
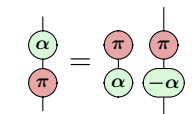
Now we give the rewriting rules of algebraic ZX-calculus.



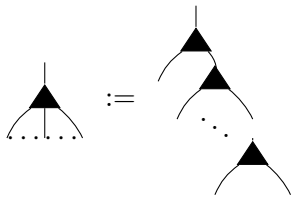
Where $a, b \in \mathbb{C}$. The vertically flipped versions of the rules are assumed to hold as well.

2.5 Useful lemmas

The following lemmas which will be used in the sequel can be derived from the rules.

<p>Lemma 1. [48] For $\tau, \sigma \in \{0, \pi\}$, pink spiders fuse.</p>  <p style="text-align: right;">(S1r)</p>	<p>Lemma 2. [48] Hadamard is involutive.</p>  <p style="text-align: right;">(H2)</p>
<p>Lemma 3. [48] Pink π transposes the triangle.</p> 	<p>Lemma 4. [48] Green π inverts the triangle.</p> 
<p>Lemma 5. [48] triangle stabilises $\langle 1$.</p> 	<p>Lemma 6. [48] Hopf rule.</p>  <p style="text-align: right;">(Hopf)</p>
<p>Lemma 7. [48] π copy rule. For $m \geq 0$:</p>  <p style="text-align: right;">(Pic)</p>	<p>Lemma 8. [48] π commutation rule.</p> 

Remark 9. Due to the associative rule (Aso), we can define the W spider



and give its interpretation as follows [21]:

$$\underbrace{\text{W spider}}_m = \underbrace{|0 \dots 0\rangle}_m \langle 0| + \sum_{k=1}^m \underbrace{|0 \dots 0 1 0 \dots 0\rangle}_{k-1} \langle 1|.$$

As a consequence, we have

$$\begin{aligned}
 \text{Spider with } \pi \text{ on top} &= \text{Three vertical lines with dots below} \\
 \text{Spider with } \pi \text{ on top} &= \text{Spider with } \pi \text{ on top and } \pi \text{ on left} + \text{Spider with } \pi \text{ on top and } \pi \text{ on right} + \dots
 \end{aligned}
 \tag{1}$$

For $n = 2$, the state $|01\rangle + |10\rangle$ can be represented as the quantum state corresponding to the Pauli X gate according to the map-state duality:

Lemma 10.

$$\text{Spider with } \pi \text{ on top} = \text{Spider with } \pi \text{ on top}$$

3 Differentiating ZX diagrams

In this section, we show how to differentiate any algebraic ZX diagram within algebraic ZX-calculus, and how to represent the derivative of original ZX diagrams [11] and quantum circuits in algebraic ZX as a special case. We refer to [45] for a formal definition of the categorical semantics of diagrammatic differentiation. We start by differentiating the simplest parameterised generator in original ZX-calculus: the one-legged green spider.

Lemma 11. *Suppose $f(\theta)$ is a differentiable real function of θ . Then*

$$\frac{\partial}{\partial \theta} \left[\text{Spider with } f(\theta) \text{ on top} \right] = \text{Spider with } i f'(\theta) \text{ on top and } \pi \text{ on left} + \text{Spider with } f(\theta) \text{ on top and } \pi \text{ on right}$$

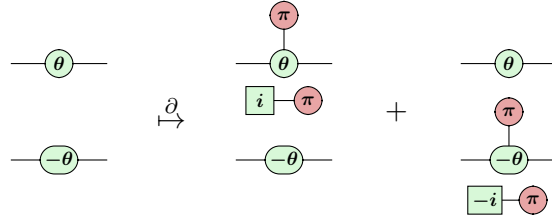
Note: For presentation purposes, the proofs of some theorems and lemmas are moved to the appendix.

Using the derivative of the one-legged spider, we can differentiate any ZX diagram with only one occurrence of the parameter being differentiated against. Here is an example.

$$\text{Spider with } 2\theta \text{ on top} = \text{Spider with } 2\theta \text{ on top} \xrightarrow{\partial} \text{Spider with } 2\theta \text{ on top and } \pi \text{ on left} + \text{Spider with } 2\theta \text{ on top and } \pi \text{ on right} \stackrel{B3}{=} \text{Spider with } 2\theta \text{ on top and } \pi \text{ on left} + \text{Spider with } 2\theta \text{ on top and } \pi \text{ on right}$$

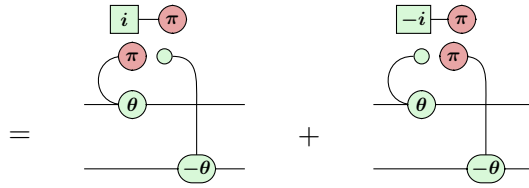
$$|00\rangle \langle 0| + e^{i2\theta} |11\rangle \langle 1| \xrightarrow{\partial} 2i * e^{i2\theta} |11\rangle \langle 1|$$

When there are multiple occurrences of the same parameter, the derivative can be expressed as a sum of ZX diagrams using the product rule. For example, the density matrix of $R_z(\theta)$ can be differentiated as follows.

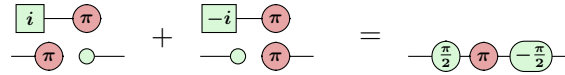


Since there are no rules on how to further manipulate sums of ZX diagrams, any reasoning from this point on would need to explicitly rely on the matrix interpretation of the diagrams instead of rewriting. In order to proceed with diagrammatic reasoning, we need to express the derivative as a single diagram.

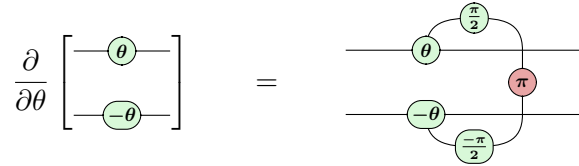
By observing that the product rule leaves the unparameterised parts of the diagram untouched and can be “factored out”, we only need to resynthesise the derivative of the parameterised part.



After this factorisation, the diagrammatic terms in the sum (top of the diagram) can be further manipulated until we can eliminate the sum using a simple rule such as $|0\rangle + |1\rangle = \sqrt{2}|+\rangle$. (See appendix for a demonstration of this technique)



Therefore



This equation, first derived by Zhao et al. [52], is essentially the parameter shift rule by Schuld et al. [40] expressed as a single ZX diagram (also see Corollary 18).

The key result of the paper allows us to express the derivative of an arbitrary ZX diagram in terms of a single diagram. It is based on the observation that the product rule and the unnormalised $|W_n\rangle$ state resemble each other: in the product rule, each term has one differentiated function, and in the W state each term has one bit set to 1 in the basis state.

$$\partial(fgh) = (\partial f)gh + f(\partial g)h + fg(\partial h)$$

$$|W_3\rangle = |100\rangle + |010\rangle + |001\rangle$$

We will show in Theorem 16 that the product rule can indeed be represented using a W state supplemented with some local change of bases. The following lemma demonstrates that the difference between f and ∂f can be expressed as a change of basis from the computational basis $|0\rangle, |1\rangle$.

Lemma 12. For any complex number a , we have

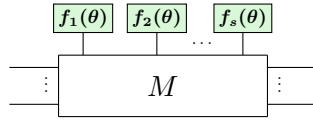


To differentiate algebraic ZX diagrams, we first differentiate its parameterised generator, the one-legged green box:

Lemma 13. *Suppose $f : \mathbb{R} \rightarrow \mathbb{C}$ is a differentiable function. Then*

$$\frac{\partial}{\partial \theta} \left[\begin{array}{c} \boxed{f(\theta)} \\ | \\ \vdots \end{array} \right] = \begin{array}{c} \boxed{f'(\theta)} \quad \pi \\ | \quad | \\ \pi \quad | \end{array}$$

All parameterised differentiable algebraic ZX diagrams can be rewritten into the following form, where M is an unparameterised ZX diagram with respect to θ , and $\{f_i(\theta)\}_i$ are differentiable real functions of θ . Parameterised green spiders can be written as a green box with an exponentiated phase, and parameterised red spiders can be converted to parameterised green spiders via Hadamard conjugation. We emphasise that M can contain other parameterised spiders, just not with respect to θ .

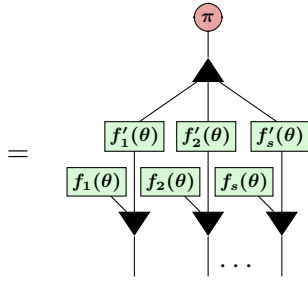


Theorem 14. *Assume $f_j : \mathbb{R} \rightarrow \mathbb{C}$ are differentiable functions. Then*

$$\frac{\partial}{\partial \theta} \left[\begin{array}{c} \boxed{f_1(\theta)} \quad \boxed{f_2(\theta)} \quad \boxed{f_s(\theta)} \\ | \quad | \quad | \\ \vdots \quad \vdots \quad \vdots \\ \boxed{M} \\ \vdots \quad \vdots \quad \vdots \end{array} \right] = \begin{array}{c} \pi \\ \swarrow \quad \downarrow \quad \searrow \\ \boxed{f'_1(\theta)} \quad \boxed{f'_2(\theta)} \quad \boxed{f'_s(\theta)} \\ | \quad | \quad | \\ \boxed{f_1(\theta)} \quad \boxed{f_2(\theta)} \quad \boxed{f_s(\theta)} \\ \vdots \quad \vdots \quad \vdots \\ \boxed{M} \\ \vdots \quad \vdots \quad \vdots \end{array}$$

Proof. By linearity, differentiating the overall diagram amounts to differentiating the parameterised part of the diagram:

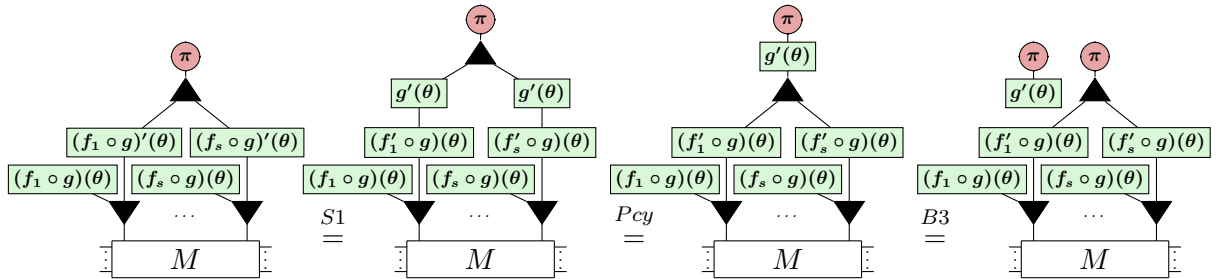
$$\begin{aligned} & \frac{\partial}{\partial \theta} \left[\begin{array}{c} \boxed{f_1(\theta)} \quad \boxed{f_2(\theta)} \quad \boxed{f_s(\theta)} \\ | \quad | \quad | \\ \vdots \quad \vdots \quad \vdots \end{array} \right] \\ &= \begin{array}{c} \boxed{f'_1(\theta)} \quad \pi \\ | \quad | \\ \pi \quad | \end{array} \begin{array}{c} \boxed{f_2(\theta)} \quad \boxed{f_s(\theta)} \\ | \quad | \\ \vdots \quad \vdots \end{array} + \begin{array}{c} \boxed{f'_2(\theta)} \quad \pi \\ | \quad | \\ \pi \quad | \end{array} \begin{array}{c} \boxed{f_1(\theta)} \quad \boxed{f_s(\theta)} \\ | \quad | \\ \vdots \quad \vdots \end{array} + \dots + \begin{array}{c} \boxed{f'_s(\theta)} \quad \pi \\ | \quad | \\ \pi \quad | \end{array} \begin{array}{c} \boxed{f_1(\theta)} \quad \boxed{f_2(\theta)} \\ | \quad | \\ \vdots \quad \vdots \end{array} \\ &= \begin{array}{c} \pi \quad \pi \quad \pi \\ \swarrow \quad \downarrow \quad \searrow \\ \boxed{f_1(\theta)} \quad \boxed{f_2(\theta)} \quad \boxed{f_s(\theta)} \\ | \quad | \quad | \\ \boxed{f'_1(\theta)} \quad \boxed{f'_2(\theta)} \quad \boxed{f'_s(\theta)} \\ | \quad | \quad | \\ \pi \quad | \quad | \end{array} + \begin{array}{c} \pi \quad \pi \quad \pi \\ \swarrow \quad \downarrow \quad \searrow \\ \boxed{f_1(\theta)} \quad \boxed{f_2(\theta)} \quad \boxed{f_s(\theta)} \\ | \quad | \quad | \\ \boxed{f'_2(\theta)} \quad \boxed{f'_3(\theta)} \quad \boxed{f'_s(\theta)} \\ | \quad | \quad | \\ \pi \quad | \quad | \end{array} + \dots + \begin{array}{c} \pi \quad \pi \quad \pi \\ \swarrow \quad \downarrow \quad \searrow \\ \boxed{f_1(\theta)} \quad \boxed{f_2(\theta)} \quad \boxed{f_s(\theta)} \\ | \quad | \quad | \\ \boxed{f'_1(\theta)} \quad \boxed{f'_2(\theta)} \quad \boxed{f'_s(\theta)} \\ | \quad | \quad | \\ \pi \quad | \quad | \end{array} \\ &= \begin{array}{c} \pi \quad \pi \quad \pi \\ \swarrow \quad \downarrow \quad \searrow \\ \boxed{f'_1(\theta)} \quad \boxed{f'_2(\theta)} \quad \boxed{f'_s(\theta)} \\ | \quad | \quad | \\ \boxed{f_1(\theta)} \quad \boxed{f_2(\theta)} \quad \boxed{f_s(\theta)} \\ \vdots \quad \vdots \quad \vdots \end{array} + \begin{array}{c} \pi \quad \pi \quad \pi \\ \swarrow \quad \downarrow \quad \searrow \\ \boxed{f'_1(\theta)} \quad \boxed{f'_2(\theta)} \quad \boxed{f'_s(\theta)} \\ | \quad | \quad | \\ \boxed{f_1(\theta)} \quad \boxed{f_2(\theta)} \quad \boxed{f_s(\theta)} \\ \vdots \quad \vdots \quad \vdots \end{array} + \dots + \begin{array}{c} \pi \quad \pi \quad \pi \\ \swarrow \quad \downarrow \quad \searrow \\ \boxed{f'_1(\theta)} \quad \boxed{f'_2(\theta)} \quad \boxed{f'_s(\theta)} \\ | \quad | \quad | \\ \boxed{f_1(\theta)} \quad \boxed{f_2(\theta)} \quad \boxed{f_s(\theta)} \\ \vdots \quad \vdots \quad \vdots \end{array} \end{aligned}$$



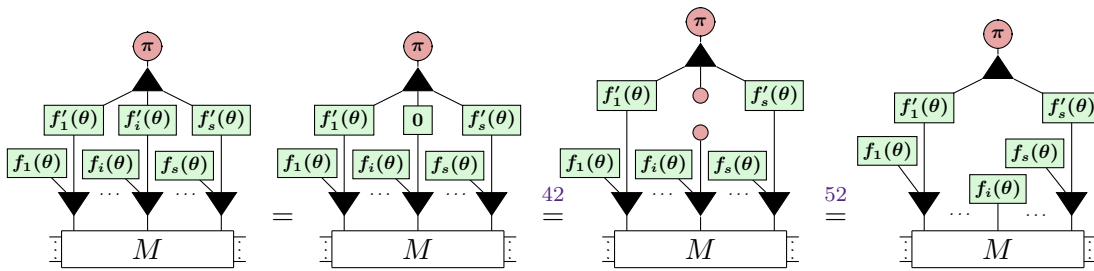
The first step follows from Lemma 13 and the product rule, the second step follows from Lemma 52 and Lemma 53, and the third step follows from the π commutation rule for green boxes. The final step uses the property of W spider as given in (1). \square

This theorem unifies the linearity and product rules of differential calculus into a single diagram, without a blowup in diagram size: the number of nodes added to the diagram after differentiation is linearly proportional to the number of parameter occurrences. This makes the result practically useful for both calculations by hand and computer simulation.

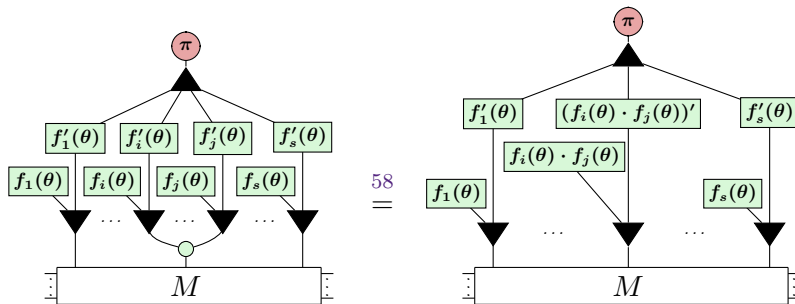
Remark 15. Using the chain rule, we can pull out a common factor if all f_i are composed with some other function g :



If f_i is a constant function, the corresponding spider does not contribute to the derivative:

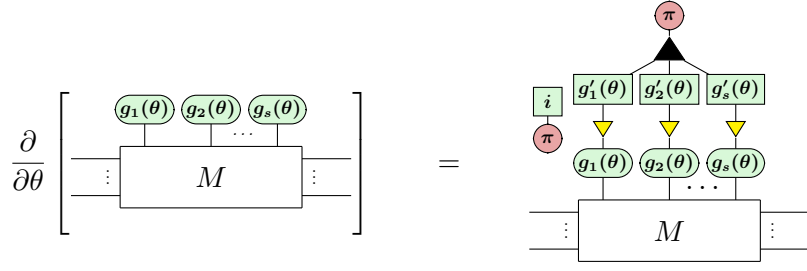


Finally, the differentiation gadget nicely interacts with spider fusion:



Diagrammatic differentiation for regular ZX diagrams corresponds to the special case where all f_j are phase functions:

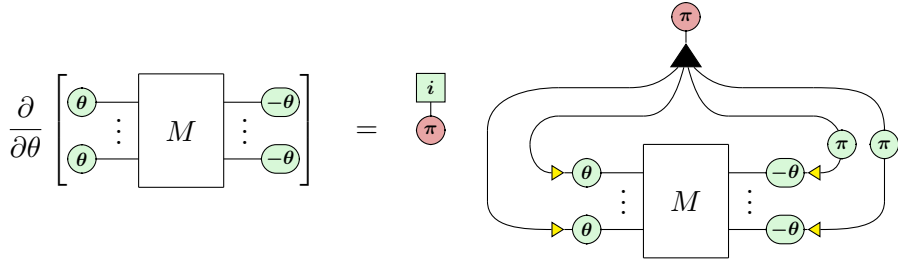
Theorem 16. *The derivative of a differentiable ZX diagram can be expressed as a single ZX diagram:*



Proof. This is a special case of Theorem 14, where $f_j(\theta) = e^{ig_j(\theta)} \neq 0$ and $\frac{f'_j(\theta)}{f_j(\theta)} = ig'_j(\theta)$, thus Lemma 57 applies. The “ i ” is common across all functions and can be factored out through the W spider using the diagrammatic chain rule from Remark 15. \square

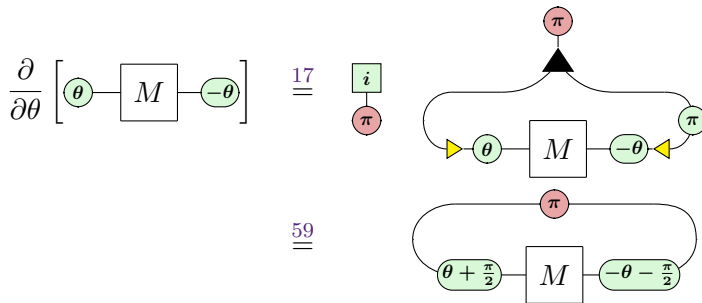
Since we can now differentiate arbitrary ZX diagrams, we can consider differentiating quantum circuits as a special case of Theorem 16. Executing a circuit $U(\theta)$ for some observable H on a quantum computer estimates the expectation value $\langle H \rangle = \langle 0 | U^\dagger(\theta) H U(\theta) | 0 \rangle$. Thus, the ZX diagram representing $\langle H \rangle$ has an equal number of occurrences of θ and $-\theta$.

Corollary 17. *The derivative of a parameterised quantum circuit can be expressed as a single ZX diagram:*



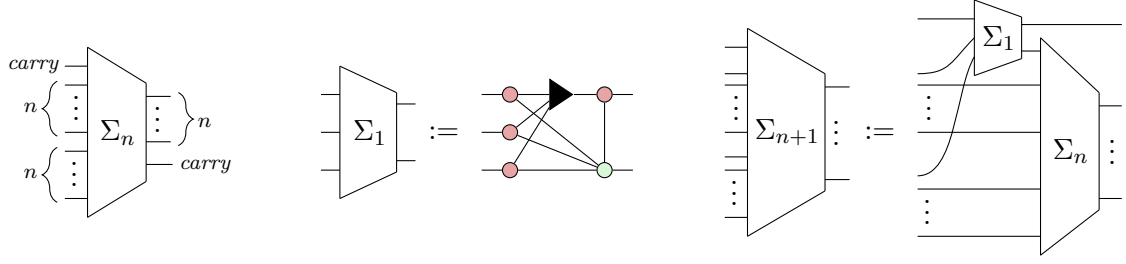
Proof. Noting that $\frac{\partial}{\partial \theta} -\theta = -1$ and $\boxed{-1} = \pi$, this follows directly from Theorem 16. \square

Corollary 18. *As a special case of Corollary 17, we obtain the parameter-shift rule from [40].*



Remark 19. *This result has been given as a theorem in [52], here we directly get it as a consequence of Corollary 17 which follows from Theorem 16.*

Definition 24. We define the diagram Σ_n recursively via

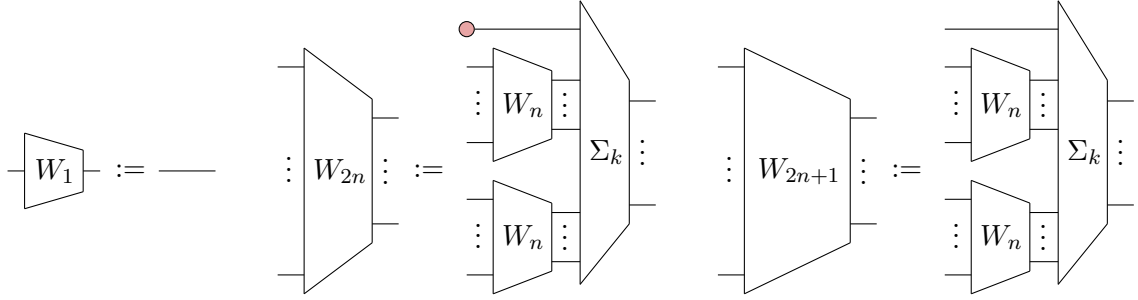


The construction of Σ_n is analogous to a classical ripple-carry adder, where Σ_1 acts as a full-adder [35]. Its action on computational basis states thus corresponds to binary addition.

Lemma 25. Σ_n performs binary addition, i.e. for all $\vec{x}, \vec{y} \in \{0, 1\}^n$ and $c \in \{0, 1\}$, we have $\Sigma_n |c, \vec{x}, \vec{y}\rangle = |\vec{z}\rangle$ where $[\vec{z}] = [\vec{x}] + [\vec{y}] + c$.

Using this adder, we define a diagram that computes the binary Hamming weight of its input using a divide-and-conquer strategy.

Definition 26. We define the diagram $n \left\{ \begin{array}{c} \vdots \\ W_n \\ \vdots \end{array} \right\}_{\lfloor \log n \rfloor + 1}$ recursively via



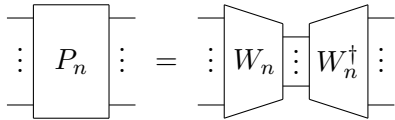
where $k = \lfloor \log n \rfloor + 1$.

Proposition 27. The diagram size of W_n only grows linearly with increasing n .

Lemma 28. W_n computes the binary Hamming weight, i.e. for all $\vec{x} \in \{0, 1\}^n$, we have $W_n |\vec{x}\rangle = |\vec{z}\rangle$ where $[\vec{z}] = w(\vec{x})$.

This immediately yields a single diagram representation of the Hamming weight projector P_n .

Corollary 29. We can represent P_n as a single diagram in terms of W_n :



Proof. Follows by comparing the action on all computational basis states. For all $\vec{x}, \vec{y} \in \{0, 1\}^n$, we have

$$\begin{array}{c} \textcircled{x_1\pi} \\ \vdots \\ \textcircled{x_n\pi} \end{array} \begin{array}{c} \vdots \\ P_n \\ \vdots \end{array} \begin{array}{c} \textcircled{y_1\pi} \\ \vdots \\ \textcircled{y_n\pi} \end{array} \stackrel{22}{=} \begin{cases} 1 & \text{if } w(\vec{x}) = w(\vec{y}) \\ 0 & \text{otherwise} \end{cases}$$

$$\begin{array}{c}
\begin{array}{c} \circlearrowleft x_1 \pi \\ \vdots \\ \circlearrowleft x_2 \pi \end{array} \begin{array}{c} \diagup \\ \vdots \\ \diagdown \end{array} W_n \begin{array}{c} \vdots \\ \vdots \\ \vdots \end{array} \begin{array}{c} \diagdown \\ \vdots \\ \diagup \end{array} W_n^\dagger \begin{array}{c} \circlearrowright y_1 \pi \\ \vdots \\ \circlearrowright y_n \pi \end{array} \\
\cong \begin{array}{c} \circlearrowleft a_1 \pi \quad \circlearrowright b_1 \pi \\ \vdots \\ \circlearrowleft a_k \pi \quad \circlearrowright b_k \pi \end{array} = \begin{cases} 1 & \text{if } \vec{a} = \vec{b} \\ 0 & \text{otherwise} \end{cases} = \begin{cases} 1 & \text{if } w(\vec{x}) = w(\vec{y}) \\ 0 & \text{otherwise} \end{cases}
\end{array}$$

where $k = \lfloor \log(n) \rfloor + 1$, $[\vec{a}] = w(\vec{x})$, and $[\vec{b}] = w(\vec{y})$. The last step follows since the binary interpretation $[\cdot]$ is a bijective mapping, so $\vec{a} = \vec{b} \iff [\vec{a}] = [\vec{b}] \iff w(\vec{x}) = w(\vec{y})$. \square

Theorem 30. Let k be a non-zero integer and M a diagram with no occurrence of θ . Then

$$\frac{1}{2\pi} \int_{-\pi}^{\pi} \begin{array}{c} n \left\{ \begin{array}{c} \circlearrowleft k\theta \\ \vdots \\ \circlearrowleft k\theta \end{array} \right\} \\ \vdots \\ m \left\{ \begin{array}{c} \vdots \\ \vdots \\ \vdots \end{array} \right\} \end{array} M \begin{array}{c} \vdots \\ \vdots \\ \vdots \end{array} \begin{array}{c} n \left\{ \begin{array}{c} \circlearrowright -k\theta \\ \vdots \\ \circlearrowright -k\theta \end{array} \right\} \\ \vdots \\ l \left\{ \begin{array}{c} \vdots \\ \vdots \\ \vdots \end{array} \right\} \end{array} d\theta = \begin{array}{c} \begin{array}{c} \vdots \\ \vdots \\ \vdots \end{array} W_n \begin{array}{c} \vdots \\ \vdots \\ \vdots \end{array} W_n^\dagger \begin{array}{c} \vdots \\ \vdots \\ \vdots \end{array} \\ \vdots \\ \begin{array}{c} \vdots \\ \vdots \\ \vdots \end{array} M \begin{array}{c} \vdots \\ \vdots \\ \vdots \end{array} \\ m \left\{ \begin{array}{c} \vdots \\ \vdots \\ \vdots \end{array} \right\} \quad l \left\{ \begin{array}{c} \vdots \\ \vdots \\ \vdots \end{array} \right\} \end{array}$$

Proof. Immediately follows from Lemma 21 and Corollary 29. \square

Similar to the differentiation diagrams from the previous section, the size of this integration diagram is linear in n (follows from Proposition 27).

4.2 General Integration

Now, we can easily extend the integration result from circuits to arbitrary ZX diagrams with a different number of positive and negative occurrences of θ .

Theorem 31. Let k be a non-zero integer, M a diagram with no occurrence of θ , and w.l.o.g. $m \leq n$. Then

$$\frac{1}{2\pi} \int_{-\pi}^{\pi} \begin{array}{c} n \left\{ \begin{array}{c} \circlearrowleft k\theta \\ \vdots \\ \circlearrowleft k\theta \end{array} \right\} \\ \vdots \\ l \left\{ \begin{array}{c} \vdots \\ \vdots \\ \vdots \end{array} \right\} \end{array} M \begin{array}{c} \vdots \\ \vdots \\ \vdots \end{array} \begin{array}{c} m \leq n \left\{ \begin{array}{c} \circlearrowright -k\theta \\ \vdots \\ \circlearrowright -k\theta \end{array} \right\} \\ \vdots \\ p \left\{ \begin{array}{c} \vdots \\ \vdots \\ \vdots \end{array} \right\} \end{array} d\theta = \begin{array}{c} \begin{array}{c} \vdots \\ \vdots \\ \vdots \end{array} W_n \begin{array}{c} \vdots \\ \vdots \\ \vdots \end{array} W_n^\dagger \begin{array}{c} \circlearrowright \dots \\ \circlearrowright \dots \end{array} \left. \begin{array}{c} \vdots \\ \vdots \\ \vdots \end{array} \right\}^{n-m} \\ \vdots \\ \begin{array}{c} \vdots \\ \vdots \\ \vdots \end{array} M \begin{array}{c} \vdots \\ \vdots \\ \vdots \end{array} \\ l \left\{ \begin{array}{c} \vdots \\ \vdots \\ \vdots \end{array} \right\} \quad p \left\{ \begin{array}{c} \vdots \\ \vdots \\ \vdots \end{array} \right\} \end{array}$$

Proof. We can rewrite the diagram into one with the same number of positive and negative occurrences of θ by exploiting the fact that $\circlearrowleft k\theta \text{---} \bullet = \circlearrowright -k\theta \text{---} \bullet = 1$.

$$\begin{array}{c} n \left\{ \begin{array}{c} \circlearrowleft k\theta \\ \vdots \\ \circlearrowleft k\theta \end{array} \right\} \\ \vdots \\ l \left\{ \begin{array}{c} \vdots \\ \vdots \\ \vdots \end{array} \right\} \end{array} M \begin{array}{c} \vdots \\ \vdots \\ \vdots \end{array} \begin{array}{c} m \leq n \left\{ \begin{array}{c} \circlearrowright -k\theta \\ \vdots \\ \circlearrowright -k\theta \end{array} \right\} \\ \vdots \\ p \left\{ \begin{array}{c} \vdots \\ \vdots \\ \vdots \end{array} \right\} \end{array} = \begin{array}{c} \left(\begin{array}{c} \circlearrowleft k\theta \\ \vdots \\ \circlearrowleft k\theta \end{array} \right) \begin{array}{c} \vdots \\ \vdots \\ \vdots \end{array} M \begin{array}{c} \vdots \\ \vdots \\ \vdots \end{array} \begin{array}{c} \left. \begin{array}{c} \circlearrowright -k\theta \\ \vdots \\ \circlearrowright -k\theta \end{array} \right\}^m \\ \vdots \\ \left. \begin{array}{c} \circlearrowleft k\theta \\ \vdots \\ \circlearrowleft k\theta \end{array} \right\}^{n-m} \end{array} \\ \vdots \\ l \left\{ \begin{array}{c} \vdots \\ \vdots \\ \vdots \end{array} \right\} \quad p \left\{ \begin{array}{c} \vdots \\ \vdots \\ \vdots \end{array} \right\} \end{array}$$

Then, the result immediately follows from Theorem 30. \square

4.3 Examples

To conclude, we explicitly give the integration diagrams for the cases $n = 1, 2, 3$ to illustrate and compare our integration approach with the work in [52].

Example 32. Let k be a non-zero integer and M a diagram with no occurrence of θ . Then

$$\frac{1}{2\pi} \int_{-\pi}^{\pi} \left(\begin{array}{c} \textcircled{k\theta} \quad \textcircled{-k\theta} \\ \vdots \\ M \\ \vdots \\ \textcircled{k\theta} \quad \textcircled{-k\theta} \end{array} \right)_n d\alpha \stackrel{30}{=} \left(\begin{array}{c} \text{---} \\ \vdots \\ M \\ \vdots \\ \text{---} \end{array} \right)_n$$

This equation has been proved in [52] for $k = 1$. Here we obtain the result directly from Theorem 30 using the fact that W_1 is the identity.

Example 33. Let k be a non-zero integer and M a diagram with no occurrence of θ . Then

$$\frac{1}{2\pi} \int_{-\pi}^{\pi} \left(\begin{array}{c} \textcircled{k\theta} \quad \textcircled{-k\theta} \\ \textcircled{k\theta} \quad \textcircled{-k\theta} \\ \vdots \\ M \\ \vdots \\ \textcircled{k\theta} \quad \textcircled{-k\theta} \end{array} \right)_n d\theta \stackrel{30}{=} \left(\begin{array}{c} \text{---} \\ \vdots \\ M \\ \vdots \\ \text{---} \end{array} \right)_n \stackrel{67}{=} \left(\begin{array}{c} \text{---} \\ \vdots \\ M \\ \vdots \\ \text{---} \end{array} \right)_n$$

The corresponding result of this theorem is shown as Lemma 2 in [52] where there are three diagrammatic sum terms after integration, which results in their computation of variance of gradients becoming rather complicated. Here we only obtain a single diagram after integration.

Example 34. Let k be a non-zero integer and M a diagram with no occurrence of θ . Then

$$\frac{1}{2\pi} \int_{-\pi}^{\pi} \left(\begin{array}{c} \textcircled{k\theta} \quad \textcircled{-k\theta} \\ \textcircled{k\theta} \quad \textcircled{-k\theta} \\ \textcircled{k\theta} \quad \textcircled{-k\theta} \\ \vdots \\ M \\ \vdots \\ \textcircled{k\theta} \quad \textcircled{-k\theta} \end{array} \right)_n d\theta \stackrel{30}{=} \left(\begin{array}{c} \text{---} \\ \vdots \\ M \\ \vdots \\ \text{---} \end{array} \right)_n$$

Zhao and Gao only considered diagrams with up to 2 occurrences of $\pm\theta$, so an equivalent result does not exist in [52].

5 Example Application: Quantum Machine Learning

In the NISQ era of quantum computing [39], many applications require the optimisation of parameterised quantum circuits: in quantum chemistry, variational quantum eigensolvers [33] are optimised to find the ground state of a Hamiltonian; in quantum machine learning, a circuit ansatz is optimised against a cost function [32], much alike how neural networks are optimised in classical machine learning.

However, while the approach of using gradient-based methods to optimise deep neural networks has been consistently effective [9], gradient-based optimisation of parameterised quantum circuits often suffer from barren plateaus: the training landscape of many circuit ansätze have been shown to be exponentially flat with respect to circuit size, making gradient descent impossible [37]. Therefore, it is crucial to develop techniques to detect and avoid barren plateaus.

So far, there has not been a fully diagrammatic analysis of barren plateaus using ZX-calculus. We believe the main obstacle to the analysis is the lack of techniques for manipulating sums of diagrams: an expectation of a Hamiltonian contains at least two occurrences of each circuit parameter, so the derivative of the expectation with respect to that parameter requires the product rule. Similarly, the rule for integrating diagrams in [52] introduces three terms, after n integrals there would be 3^n terms. Using these rules, the analysis of barren plateaus becomes exponentially costly, as the number of diagrams to be evaluated is exponential to the number of parameters in the circuit.

In this section, as a demonstration of the new differentiation and integration techniques of this paper, we show that the analysis of barren plateaus by Zhao et al. [52] can be done entirely within the framework of ZX without introducing sums of diagrams. Using the same setup, we consider an n -qubit parameterised quantum circuit $U(\boldsymbol{\theta})$ and a Hamiltonian H , obtaining the expectation value $\langle H \rangle = \langle 0 | U^\dagger(\boldsymbol{\theta}) H U(\boldsymbol{\theta}) | 0 \rangle$. If $\mathbf{Var} \left(\frac{\partial \langle H \rangle}{\partial \theta_j} \right) \approx 0$ for all j , then the quantum circuit is likely to start in a barren plateau where the circuit gradients $\frac{\partial \langle H \rangle}{\partial \theta_j}$ are close to 0.

5.1 Method

Similar to Zhao et al. [52], we make some assumptions on the circuit $U(\boldsymbol{\theta})$:

1. The parameterised gates in U are R_X , R_Y , or R_Z and do not share parameters.
2. The parameters $\boldsymbol{\theta}$ are independently and uniformly distributed on the interval $[\pi, -\pi]$.

This allows us to represent $U(\boldsymbol{\theta})$ as a ZX diagram where each parameter θ_j only occurs once. Thus, we can use the following notation for the expectation value $\langle H \rangle = \langle 0 | U^\dagger(\boldsymbol{\theta}) H U(\boldsymbol{\theta}) | 0 \rangle$ where the parametrised spiders are fused out.

$$\langle H \rangle = \begin{array}{ccc} \textcircled{\theta_1} & \text{---} & \text{---} & \textcircled{-\theta_1} \\ \vdots & & & \vdots \\ \textcircled{\theta_m} & \text{---} & E_H & \text{---} & \textcircled{-\theta_m} \end{array} \quad (2)$$

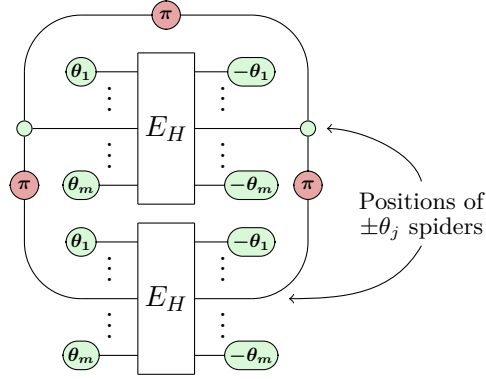
Lemma 35. [52] *Given $\langle H \rangle$ in the form of (2), we have $\mathbf{E} \left(\frac{\partial \langle H \rangle}{\partial \theta_j} \right) = 0$, for $j = 1, \dots, m$.*

As a consequence, we have

$$\begin{aligned} \mathbf{Var} \left(\frac{\partial \langle H \rangle}{\partial \theta_j} \right) &= \mathbf{E} \left(\left(\frac{\partial \langle H \rangle}{\partial \theta_j} \right)^2 \right) \\ &= \frac{1}{(2\pi)^m} \int_{-\pi}^{\pi} \cdots \int_{-\pi}^{\pi} \left(\frac{\partial \langle H \rangle}{\partial \theta_j} \right)^2 d\theta_1 \cdots d\theta_m, j = 1, \dots, m. \end{aligned}$$

Note that we can use squares here since the expectation value $\langle H \rangle$ is a real variable.

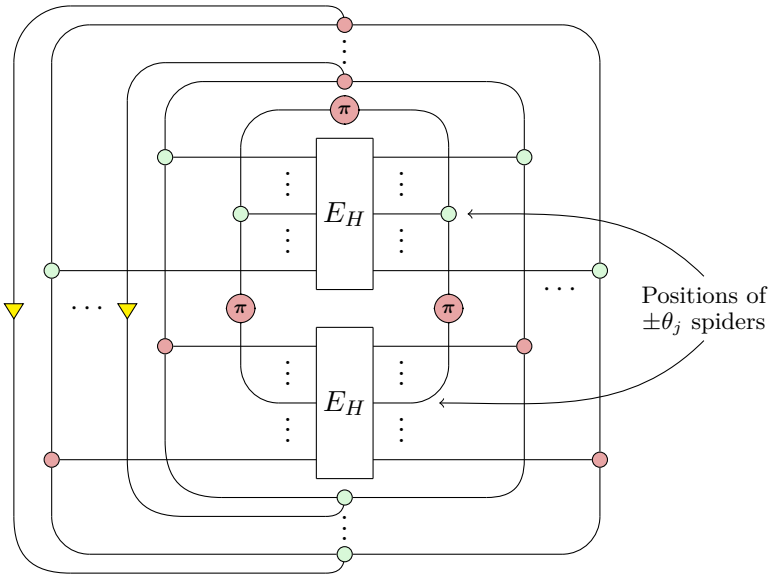
Lemma 36. [52] Given $\langle H \rangle$ in the form of (2), we have

$$\frac{1}{2\pi} \int_{-\pi}^{\pi} \left(\frac{\partial \langle H \rangle}{\partial \theta_j} \right)^2 d\theta_j =$$


where the cycle connects the legs of E_H that correspond to the positions of the $\pm\theta_j$ spiders in (2).

Remark 37. An equivalent version of this lemma is given on page 12 in [52]. Here, we obtain the result using our general differentiation and integration method.

Theorem 38. Given $\langle H \rangle$ in the form of (2), we have

$$\text{Var} \left(\frac{\partial \langle H \rangle}{\partial \theta_j} \right) =$$


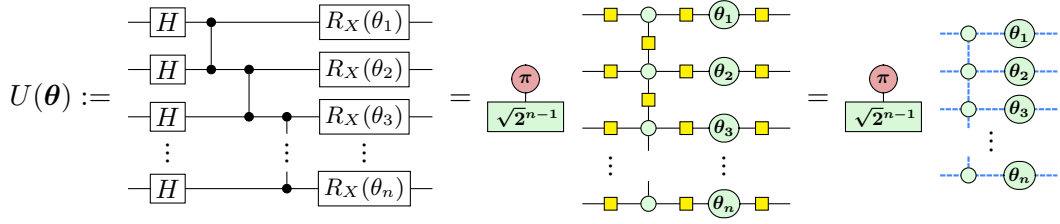
Proof. We start from the diagram as shown in Lemma 36, then drag out variables iteratively according to Example 33, and the result follows. \square

Remark 39. The variance computed in [52] is based on a sum over 3^{m-1} terms (m is the number of parameters in the considered circuit), so when m is large it becomes infeasible to analyse the variance purely within ZX. Thus they have to resort to tensor networks which goes beyond the ZX method. In contrast, we avoid this exponential explosion by integrating without sums using algebraic ZX-calculus.

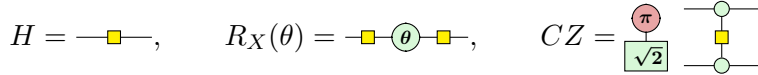
5.2 Example

Finally, we demonstrate Theorem 38 by analysing an example ansatz for the existence of barren plateaus. Concretely, we study the following n -qubit hardware efficient ansatz from [42], which

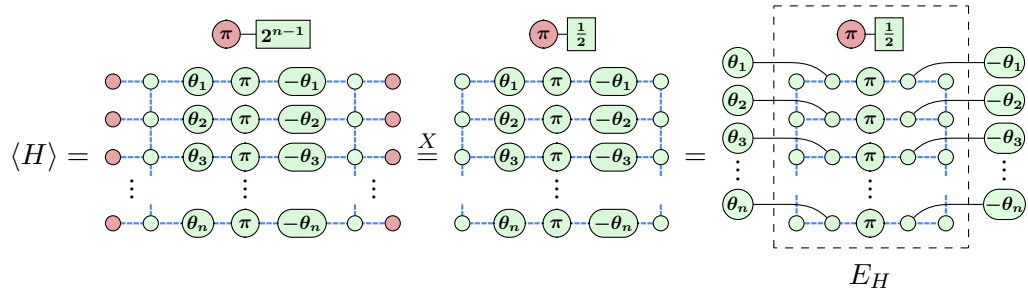
to the best of our knowledge has not been analysed before.



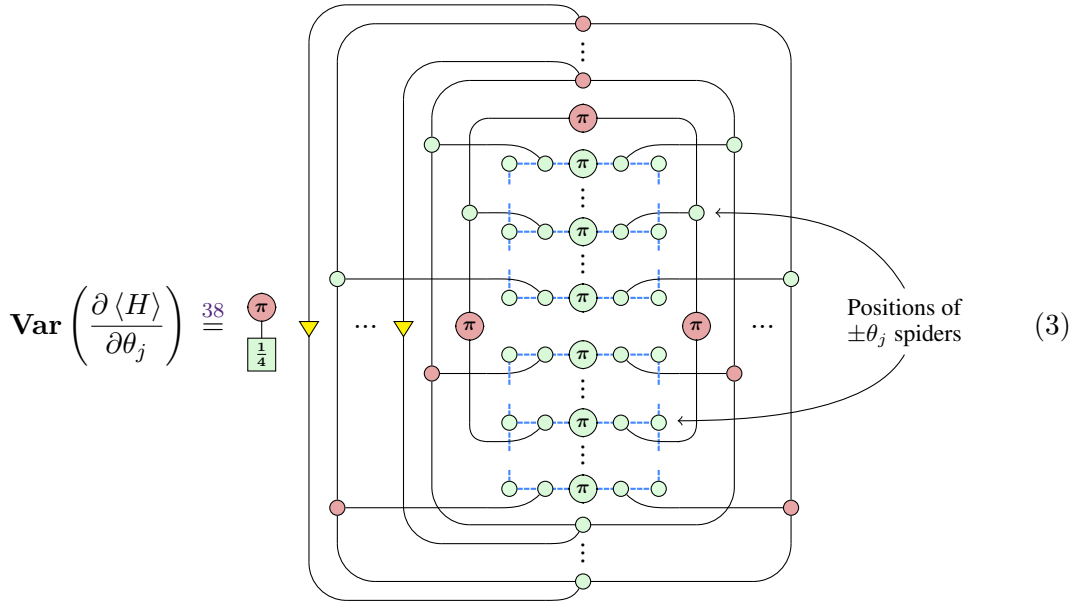
Here, we used the standard ZX representation of quantum gates, i.e.



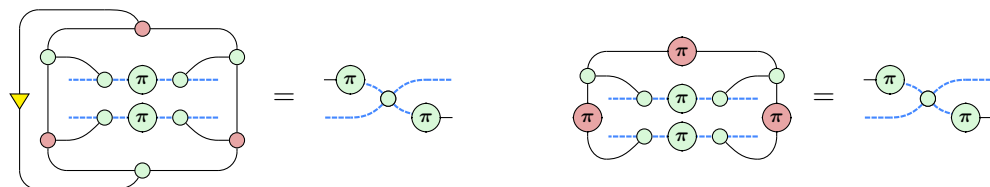
and we used blue dashed lines to denote wires with a Hadamard gate on them. For this example, we will consider the Hamiltonian $H = Z^{\otimes n}$ which corresponds to measuring all qubits in the computational basis. This gives us



Now, we can use Theorem 38 to get a single ZX diagram that represents the variance of $\langle H \rangle$'s gradient w.r.t. some parameter θ_j .

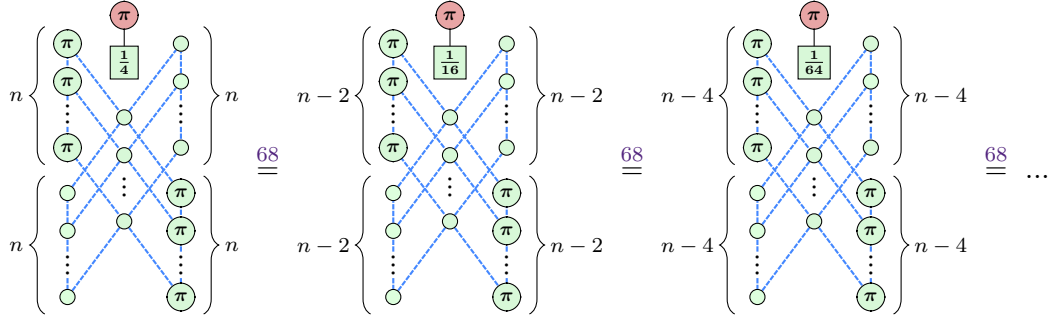


Lemma 40. *The cycles in diagram (3) can be broken up as follows.*



Proposition 41. *The ansatz $U(\theta)$ suffers from barren plateaus for $H = Z^{\otimes n}$.*

Proof. Using Lemma 40, we simplify the variance diagram (3) to



The initial diagram contains $5n$ spiders connected by Hadamard edges. We repeatedly apply Lemma 68, each time reducing the number of spiders by 10 and collecting a scalar of $\frac{1}{4}$. Depending on the parity of n , we will end up with 5 or 10 spiders scaled by $\frac{1}{2^n}$. Since the final diagram size is constant in n , we can conclude that the overall scaling is in $O\left(\frac{1}{2^n}\right)$. Thus, $U(\theta)$ suffers from barren plateaus. \square

Our diagrammatic differentiation and integration approach allowed us to carry out this analysis purely using simple reasoning and rewriting on polynomially-sized ZX diagrams. Compared to Zhao et al. [52], we did not need to resort to general tensor networks or consider diagrams with an exponential number of terms or exponential size.

For more advanced examples of barren plateau detection using Theorem 38 we refer to [30] where more ansätze from [42] as well as IQP ansätze [41] are analysed using our approach.

6 Conclusion and further work

We have elevated ZX-calculus from a graphical language for algebraic calculations to a new graphical tool for analytical reasoning. For example, it can now be used for tackling quantum optimisation problems and reasoning about quantum mechanics. We believe these techniques will extend the applicability of ZX-calculus to more problems related to quantum computing. With more work, ZX-calculus can become a general tool for graphical differential calculus.

There are many directions for future work:

1. **Generalisation of the results to qudit and qfinite cases [50]:** The ideas in this paper can be extended beyond qubits, giving us more diagrammatic analytical tools.
2. **Indefinite integration:** This paper only gives the definite integral for ZX diagrams between $\pm\pi$. Indefinite integration of arbitrary ZX diagrams would in a sense complete the analytical ZX-calculus.
3. **Parameter shift rules:** As pointed out in Corollary 18, we recovered a graphical version of the parameter shift rule from [40]. Our diagrammatic approach might prove useful to discover more general shift rules or other gradient computation methods. See [30] for some initial investigations in this area.
4. **Numerical barren plateau detection:** Since the diagram in Theorem 38 is mostly Clifford, we can use stabiliser decomposition methods [28, 29] to evaluate it. As shown in [31], this allows us to numerically detect barren plateaus more efficiently than previous sampling-based methods.

References

- [1] Gian-Luca R Anselmetti, David Wierichs, Christian Gogolin & Robert M Parrish (2021): *Local, expressive, quantum-number-preserving VQE ansätze for fermionic systems*. *New Journal of Physics* 23(11), p. 113010. Available at <https://doi.org/10.1088/1367-2630/ac2cb3>.
- [2] Miriam Backens & Ali Nabi Duman (2015): *A Complete Graphical Calculus for Spekkens' Toy Bit Theory*. *Foundations of Physics* 46(1), p. 70–103. Available at <https://doi.org/10.1007/s10701-015-9957-7>.
- [3] Miriam Backens & Aleks Kissinger (2018): *ZH: A Complete Graphical Calculus for Quantum Computations Involving Classical Non-linearity*. In: *Proceedings of the 15th International Workshop on Quantum Physics and Logic, QPL 2018, Halifax, Canada, 3-7th June 2018.*, pp. 23–42. Available at <https://doi.org/10.4204/EPTCS.287.2>.
- [4] Niel de Beaudrap, Xiaoning Bian & Quanlong Wang (2020): *Fast and Effective Techniques for T-Count Reduction via Spider Nest Identities*. In Steven T. Flammia, editor: *15th Conference on the Theory of Quantum Computation, Communication and Cryptography (TQC 2020), Leibniz International Proceedings in Informatics (LIPIcs)* 158, Schloss Dagstuhl–Leibniz-Zentrum für Informatik, Dagstuhl, Germany, pp. 11:1–11:23. Available at <https://doi.org/10.4230/LIPIcs.TQC.2020.11>.
- [5] Niel de Beaudrap, Xiaoning Bian & Quanlong Wang (2020): *Techniques to reduce $\pi/4$ -parity-phase circuits, motivated by the ZX calculus*. *Proceedings of the 16th International Conference on Quantum Physics and Logic 2019, EPTCS* 318, pp. 131–149. Available at <https://doi.org/10.4204/EPTCS.318.9>.
- [6] Niel de Beaudrap & Dominic Horsman (2020): *The ZX calculus is a language for surface code lattice surgery*. *Quantum* 4. Available at <https://doi.org/10.22331/q-2020-01-09-218>.
- [7] Jon Louis Bentley, Dorothea Haken & James B. Saxe (1980): *A general method for solving divide-and-conquer recurrences*. *SIGACT News* 12(3), p. 36–44. Available at <https://doi.org/10.1145/1008861.1008865>.
- [8] Héctor Bombín, Chris Dawson, Ryan V. Mishmash, Naomi Nickerson, Fernando Pastawski & Sam Roberts (2023): *Logical Blocks for Fault-Tolerant Topological Quantum Computation*. *PRX Quantum* 4, p. 020303. Available at <https://doi.org/10.1103/PRXQuantum.4.020303>.
- [9] Anna Choromanska, Mikael Henaff, Michael Mathieu, Gerard Ben Arous & Yann LeCun (2015): *The Loss Surfaces of Multilayer Networks*. In Guy Lebanon & S. V. N. Vishwanathan, editors: *Proceedings of the Eighteenth International Conference on Artificial Intelligence and Statistics, Proceedings of Machine Learning Research* 38, PMLR, San Diego, California, USA, pp. 192–204. Available at <https://proceedings.mlr.press/v38/choromanska15.html>.
- [10] Bob Coecke & Ross Duncan (2008): *Interacting Quantum Observables*. In: *Automata, Languages and Programming*, 5126, Springer Berlin Heidelberg, pp. 298–310. Available at https://doi.org/10.1007/978-3-540-70583-3_25.

- [11] Bob Coecke & Ross Duncan (2011): *Interacting quantum observables: categorical algebra and diagrammatics*. *New Journal of Physics* 13(4), p. 043016. Available at <https://doi.org/10.1088/1367-2630/13/4/043016>.
- [12] Bob Coecke, Ross Duncan, Aleks Kissinger & Quanlong Wang (2012): *Strong Complementarity and Non-locality in Categorical Quantum Mechanics*. In: *Proceedings of the 2012 27th Annual IEEE/ACM Symposium on Logic in Computer Science, LICS '12*, IEEE Computer Society, pp. 245–254. Available at <https://doi.org/10.1109/LICS.2012.35>.
- [13] Bob Coecke & Bill Edwards (2012): *Spekkens's toy theory as a category of processes*. *Proceedings of Symposia in Applied Mathematics* 71, pp. 61–88. Available at <https://doi.org/10.1090/psapm/071>.
- [14] Bob Coecke, Giovanni de Felice, Konstantinos Meichanetzidis & Alexis Toumi (2020): *Foundations for Near-Term Quantum Natural Language Processing*. Available at <https://doi.org/10.48550/arXiv.2012.03755>.
- [15] Bob Coecke, Dominic Horsman, Aleks Kissinger & Quanlong Wang (2022): *Kindergarten quantum mechanics graduates ...or how I learned to stop gluing LEGO together and love the ZX-calculus*. *Theoretical Computer Science* 897, pp. 1–22. Available at <https://doi.org/10.1016/j.tcs.2021.07.024>.
- [16] Bob Coecke & Aleks Kissinger (2010): *The Compositional Structure of Multipartite Quantum Entanglement*. In Samson Abramsky, Cyril Gavoille, Claude Kirchner, Friedhelm Meyer auf der Heide & Paul G. Spirakis, editors: *Automata, Languages and Programming*, Springer Berlin Heidelberg, Berlin, Heidelberg, pp. 297–308. Available at https://doi.org/10.1007/978-3-642-14162-1_25.
- [17] Bob Coecke, Aleks Kissinger, Alex Merry & Shibdas Roy (2011): *The GHZ/W-calculus contains rational arithmetic*. *Electronic Proceedings in Theoretical Computer Science* 52, p. 34–48. Available at <https://doi.org/10.4204/eptcs.52.4>.
- [18] Ross Duncan, Aleks Kissinger, Simon Perdrix & John Van De Wetering (2020): *Graph-theoretic Simplification of Quantum Circuits with the ZX-calculus*. *Quantum* 4, p. 279. Available at <https://doi.org/10.22331/q-2020-06-04-279>.
- [19] Ross Duncan & Simon Perdrix (2010): *Rewriting measurement-based quantum computations with generalised flow*. In: *International Colloquium on Automata, Languages, and Programming*, Springer, pp. 285–296. Available at https://doi.org/10.1007/978-3-642-14162-1_24.
- [20] Stefano Gogioso & William Zeng (2019): *Generalised Mermin-type non-locality arguments*. *Logical Methods in Computer Science* Volume 15, Issue 2. Available at [https://doi.org/10.23638/LMCS-15\(2:3\)2019](https://doi.org/10.23638/LMCS-15(2:3)2019).
- [21] A. Hadzihanovic (2015): *A Diagrammatic Axiomatisation for Qubit Entanglement*. In: *2015 30th Annual ACM/IEEE Symposium on Logic in Computer Science (LICS)*, IEEE Computer Society, Los Alamitos, CA, USA, pp. 573–584. Available at <https://doi.org/10.1109/LICS.2015.59>.
- [22] Amar Hadzihanovic (2015): *A Diagrammatic Axiomatisation for Qubit Entanglement*. In: *2015 30th Annual ACM/IEEE Symposium on Logic in Computer Science*, pp. 573–584. Available at <https://doi.org/10.1109/LICS.2015.59>.

- [23] Amar Hadzihasanovic, Kang Feng Ng & Quanlong Wang (2018): *Two Complete Axiomatisations of Pure-state Qubit Quantum Computing*. In: *Proceedings of the 33rd Annual ACM/IEEE Symposium on Logic in Computer Science, LICS '18*, ACM, pp. 502–511. Available at <https://doi.org/10.1145/3209108.3209128>.
- [24] Emmanuel Jeandel, Simon Perdrix & Margarita Veshchezerova (2022): *Addition and Differentiation of ZX-Diagrams*. In Amy P. Felty, editor: *7th International Conference on Formal Structures for Computation and Deduction, FSCD 2022, August 2-5, 2022, Haifa, Israel, LIPIcs 228*, Schloss Dagstuhl - Leibniz-Zentrum für Informatik, pp. 13:1–13:19. Available at <https://doi.org/10.4230/LIPIcs.FSCD.2022.13>.
- [25] Dimitri Kartsaklis, Ian Fan, Richie Yeung, Anna Pearson, Robin Lorenz, Alexis Toumi, Giovanni de Felice, Konstantinos Meichanetzidis, Stephen Clark & Bob Coecke (2021): *lambeq: An Efficient High-Level Python Library for Quantum NLP*. *arXiv preprint arXiv:2110.04236*. Available at <https://doi.org/10.48550/arXiv.2110.04236>.
- [26] Aleks Kissinger (2022): *Phase-free ZX diagrams are CSS codes (... or how to graphically grok the surface code)*. *arXiv preprint arXiv:2204.14038*. Available at <https://doi.org/10.48550/arXiv.2204.14038>.
- [27] Aleks Kissinger & John van de Wetering (2019): *Universal MBQC with generalised parity-phase interactions and Pauli measurements*. *Quantum* 3. Available at <https://doi.org/10.22331/q-2019-04-26-134>.
- [28] Aleks Kissinger & John van de Wetering (2022): *Simulating quantum circuits with ZX-calculus reduced stabiliser decompositions*. *Quantum Science and Technology*. Available at <https://doi.org/10.1088/2058-9565/ac5d20>.
- [29] Aleks Kissinger, John van de Wetering & Renaud Vilmart (2022): *Classical Simulation of Quantum Circuits with Partial and Graphical Stabiliser Decompositions* 232, pp. 5:1–5:13. Available at <https://doi.org/10.4230/LIPIcs.TQC.2022.5>.
- [30] Mark Koch (2022): *Quantum Machine Learning using the ZXW-Calculus*. *arXiv preprint arXiv:2210.11523*. Available at <https://doi.org/10.48550/arXiv.2210.11523>.
- [31] Mark Koch, Richie Yeung & Quanlong Wang (2024): *Contraction of ZX Diagrams with Triangles via Stabiliser Decompositions*. *Physica Scripta*. Available at <https://doi.org/10.1088/1402-4896/ad6fd8>.
- [32] Maciej Lewenstein (1994): *Quantum perceptrons*. *Journal of Modern Optics* 41(12), pp. 2491–2501. Available at <https://doi.org/10.1080/09500349414552331>.
- [33] Jin-Guo Liu, Yi-Hong Zhang, Yuan Wan & Lei Wang (2019): *Variational quantum eigensolver with fewer qubits*. *Phys. Rev. Research* 1, p. 023025. Available at <https://doi.org/10.1103/PhysRevResearch.1.023025>.
- [34] Robin Lorenz, Anna Pearson, Konstantinos Meichanetzidis, Dimitri Kartsaklis & Bob Coecke (2023): *Qnlp in practice: Running compositional models of meaning on a quantum computer*. *Journal of Artificial Intelligence Research* 76. Available at <https://doi.org/10.1613/jair.1.14329>.
- [35] M Morris Mano (1972): *Digital logic and computer design*. Prentic-Hall. ISBN: 978-0-13-214510-7.

- [36] Enrique Cervero Martín, Kirill Plekhanov & Michael Lubasch (2023): *Barren plateaus in quantum tensor network optimization*. *Quantum* 7, p. 974. Available at <https://doi.org/10.22331/q-2023-04-13-974>.
- [37] Jarrod R McClean, Sergio Boixo, Vadim N Smelyanskiy, Ryan Babbush & Hartmut Neven (2018): *Barren plateaus in quantum neural network training landscapes*. *Nature communications* 9(1), pp. 1–6. Available at <https://doi.org/10.1038/s41467-018-07090-4>.
- [38] Anthony Munson, Bob Coecke & Quanlong Wang (2020): *AND-gates in ZX-calculus: spider nest identities and QBC-completeness*. *Proceedings of the 17th International Conference on Quantum Physics and Logic (QPL) 2020*. Available at <https://doi.org/10.4204/EPTCS.340.12>.
- [39] John Preskill (2018): *Quantum Computing in the NISQ era and beyond*. *Quantum* 2, p. 79. Available at <https://doi.org/10.22331/q-2018-08-06-79>.
- [40] Maria Schuld, Ville Bergholm, Christian Gogolin, Josh Izaac & Nathan Killoran (2019): *Evaluating analytic gradients on quantum hardware*. *Physical Review A* 99(3), p. 032331. Available at <https://doi.org/10.1103/PhysRevA.99.032331>.
- [41] Dan Shepherd & Michael J Bremner (2009): *Temporally unstructured quantum computation*. *Proceedings of the Royal Society A: Mathematical, Physical and Engineering Sciences* 465(2105), pp. 1413–1439. Available at <https://doi.org/10.1098/rspa.2008.0443>.
- [42] Sukin Sim, Peter D Johnson & Alán Aspuru-Guzik (2019): *Expressibility and entangling capability of parameterized quantum circuits for hybrid quantum-classical algorithms*. *Advanced Quantum Technologies* 2(12), p. 1900070. Available at <https://doi.org/10.1002/qute.201900070>.
- [43] Seyon Sivarajah, Silas Dilkes, Alexander Cowtan, Will Simmons, Alec Edgington & Ross Duncan (2020): *t|ket>: a retargetable compiler for NISQ devices*. *Quantum Science and Technology* 6(1), p. 014003. Available at <https://doi.org/10.1088/2058-9565/ab8e92>.
- [44] Tobias Stollenwerk & Stuart Hadfield (2022): *Diagrammatic Analysis for Parameterized Quantum Circuits*. *Proceedings of the 19th International Conference on Quantum Physics and Logic (QPL)*. Available at <https://doi.org/10.4204/EPTCS.394.15>.
- [45] Alexis Toumi, Richie Yeung & Giovanni de Felice (2021): *Diagrammatic Differentiation for Quantum Machine Learning*. In Chris Heunen & Miriam Backens, editors: *Proceedings 18th International Conference on Quantum Physics and Logic, QPL 2021, Gdansk, Poland, and online, 7-11 June 2021, EPTCS 343*, pp. 132–144. Available at <https://doi.org/10.4204/EPTCS.343.7>.
- [46] Alejandro Villoria, Henning Basold & Alfons Laarman (2024): *Enriching Diagrams with Algebraic Operations*. In: *International Conference on Foundations of Software Science and Computation Structures*, Springer, pp. 121–143. Available at https://doi.org/10.1007/978-3-031-57228-9_7.
- [47] Quanlong Wang (2020): *An algebraic axiomatisation of ZX-calculus*. *Proceedings of the 17th International Conference on Quantum Physics and Logic (QPL) 2020*. Available at <https://doi.org/10.4204/EPTCS.340.16>.

- [48] Quanlong Wang (2020): *Algebraic complete axiomatisation of ZX-calculus with a normal form via elementary matrix operations*. Available at <https://doi.org/10.48550/arXiv.2007.13739>.
- [49] Quanlong Wang (2020): *Completeness of algebraic ZX-calculus over arbitrary commutative rings and semirings*. *arXiv:1912.01003v3*. Available at <https://doi.org/10.48550/arXiv.1912.01003>.
- [50] Quanlong Wang (2021): *Qufinite ZX-calculus: a unified framework of qudit ZX-calculi*. Available at <https://doi.org/10.48550/arXiv.2104.06429>.
- [51] Richie Yeung (2020): *Diagrammatic Design and Study of Ansätze for Quantum Machine Learning*. *arXiv preprint arXiv:2011.11073*. Available at <https://doi.org/10.48550/arXiv.2011.11073>.
- [52] Chen Zhao & Xiao-Shan Gao (2021): *Analyzing the barren plateau phenomenon in training quantum neural networks with the ZX-calculus*. *Quantum* 5, p. 466. Available at <https://doi.org/10.22331/q-2021-06-04-466>.

A Proofs and Lemmas

In this appendix, we include all the lemmas with their proofs which have been essentially existed (up to scalars) in previous papers. The lemmas are given in the order which they appear in this paper.

Lemma 10.

Proof.

□

Lemma 11. *Suppose $f(\theta)$ is a differentiable real function of θ . Then*

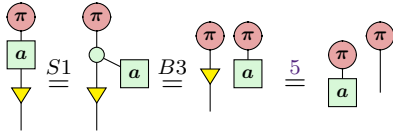
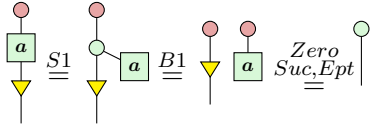
Proof.

□

Lemma 12. For any complex number a , we have

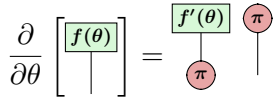


Proof.

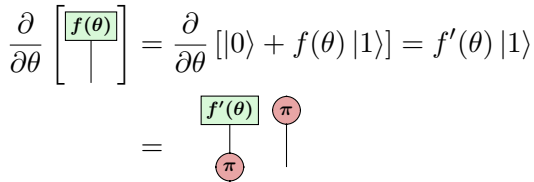


□

Lemma 13. Suppose $f : \mathbb{R} \rightarrow \mathbb{C}$ is a differentiable function. Then

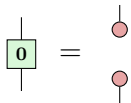


Proof.

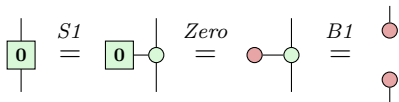


□

Lemma 42.

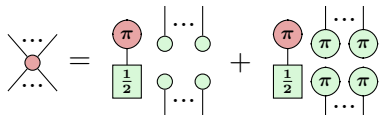


Proof.

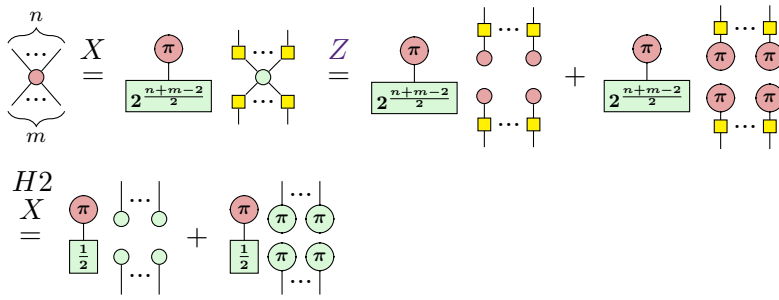


□

Lemma 43.

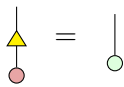


Proof.

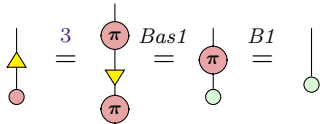


□

Lemma 44.

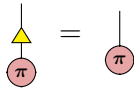


Proof.

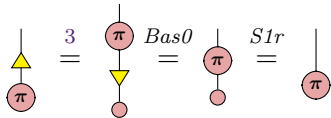


□

Lemma 45.

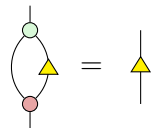


Proof.

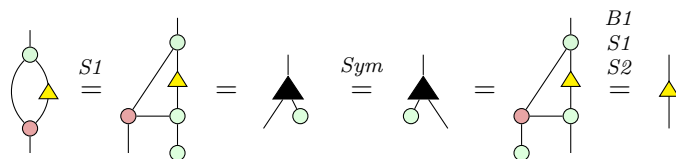


□

Lemma 46.

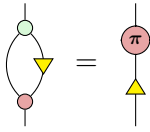


Proof.

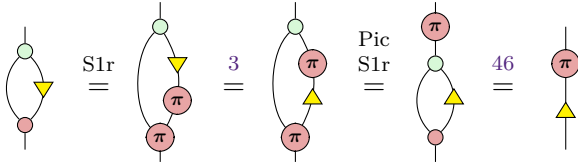


□

Lemma 47.

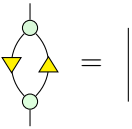


Proof.

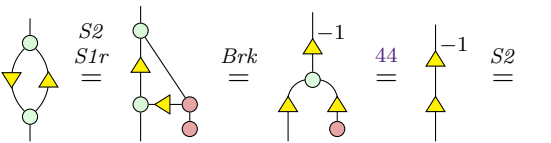


□

Lemma 48.

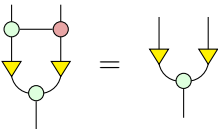


Proof.

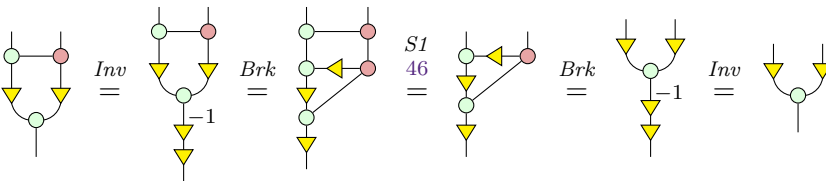


□

Lemma 49.

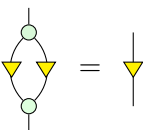


Proof.

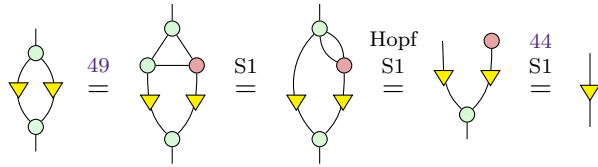


□

Lemma 50.

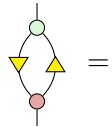


Proof.

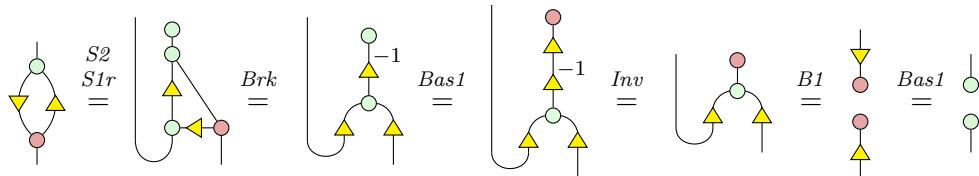


□

Lemma 51.

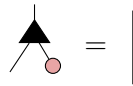


Proof.

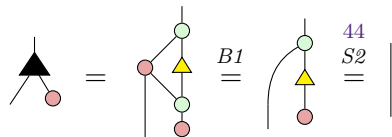


□

Lemma 52.

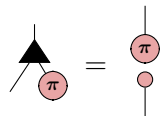


Proof.

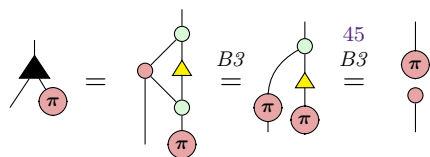


□

Lemma 53.

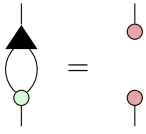


Proof.

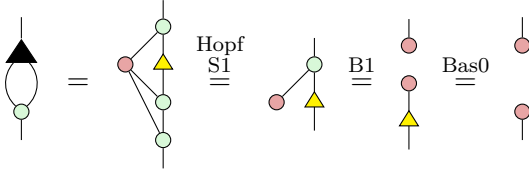


□

Lemma 54.

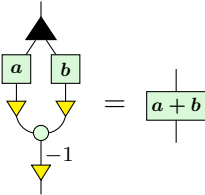


Proof.

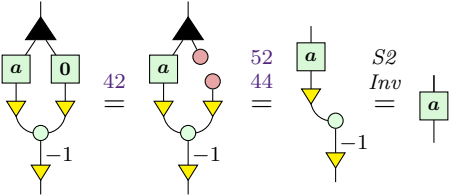


□

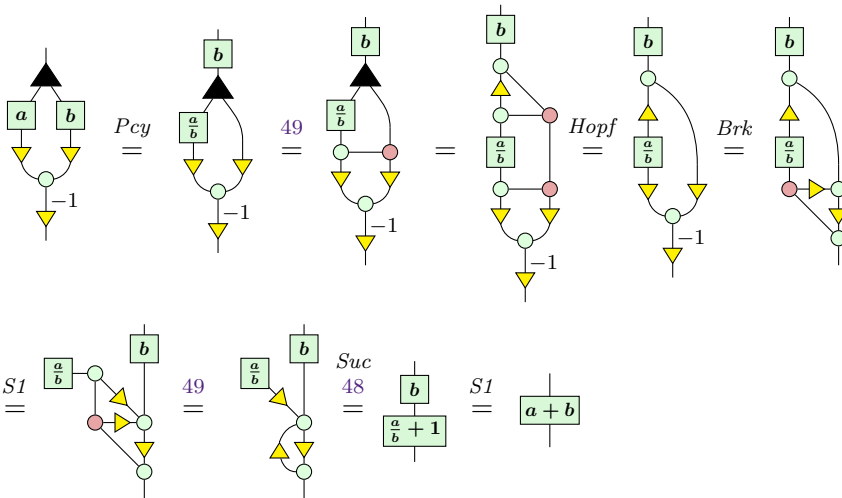
Lemma 55. Let $a, b \in \mathbb{C}$. Then



Proof. If $b = 0$, then

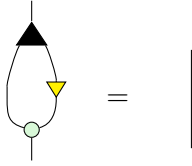


If $b \neq 0$, then

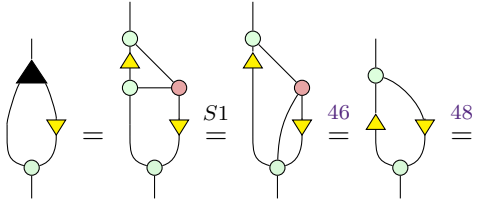


□

Lemma 56.

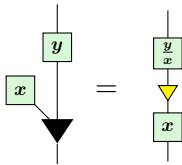


Proof.

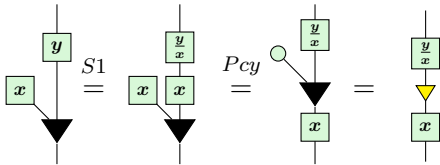


□

Lemma 57. Let $0 \neq x, y \in \mathbb{C}$. Then

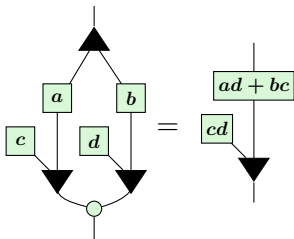


Proof.

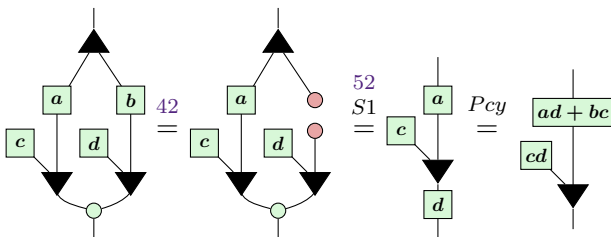


□

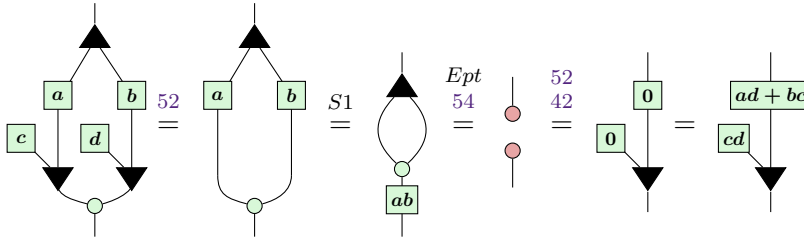
Lemma 58. Let $a, b, c, d \in \mathbb{C}$. Then



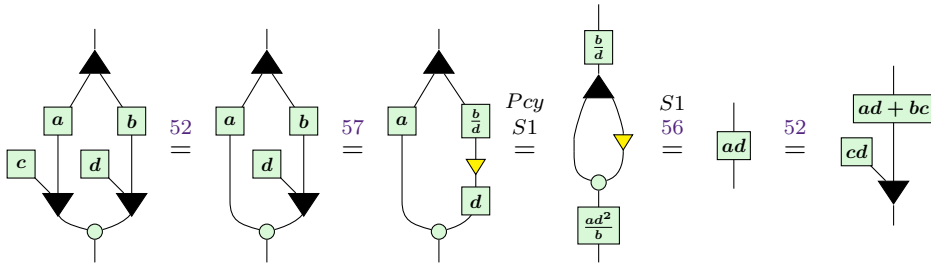
Proof. If $b = 0$, then



If $b \neq 0, c = d = 0$, then



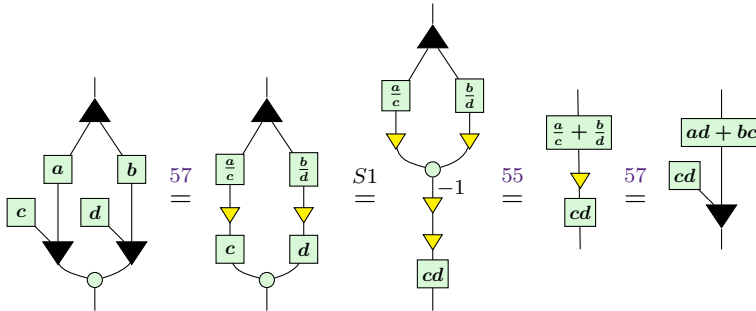
If $b \neq 0, c = 0, d \neq 0$, then



If $b \neq 0, c \neq 0, a = 0$, then the proof is similar to the case when $b = 0$.

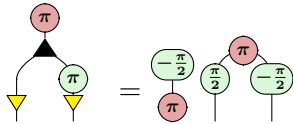
If $b \neq 0, c \neq 0, a \neq 0, d = 0$, then the proof is similar to the case when $b \neq 0, c = 0, d \neq 0$.

If $b \neq 0, c \neq 0, a \neq 0, d \neq 0$, then

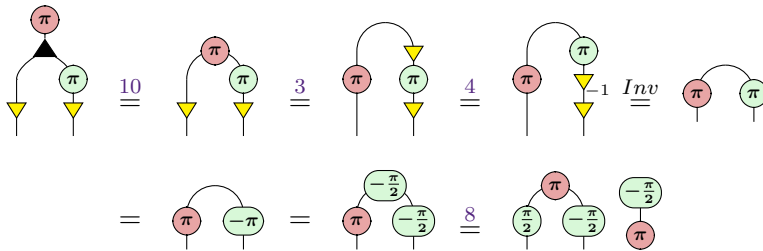


□

Lemma 59.

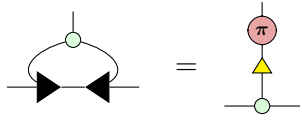


Proof.

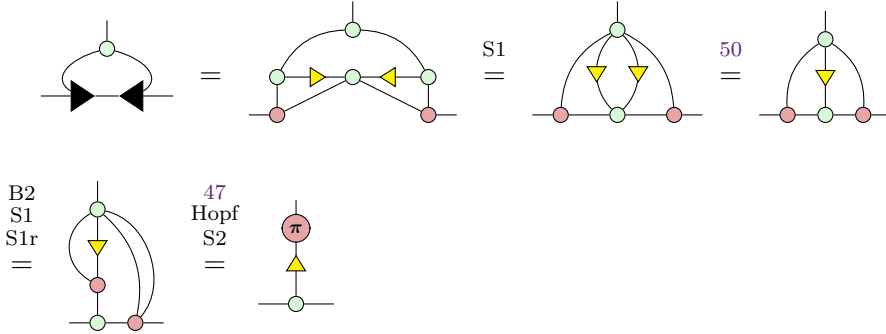


□

Lemma 60.

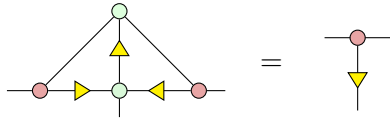


Proof.

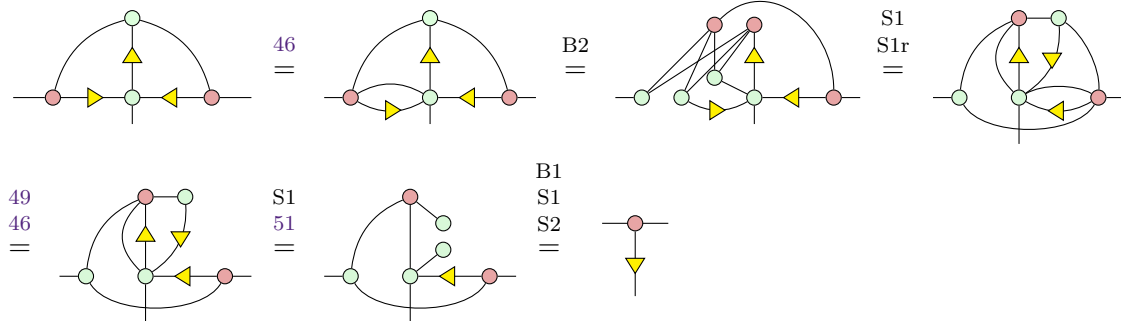


□

Lemma 61.



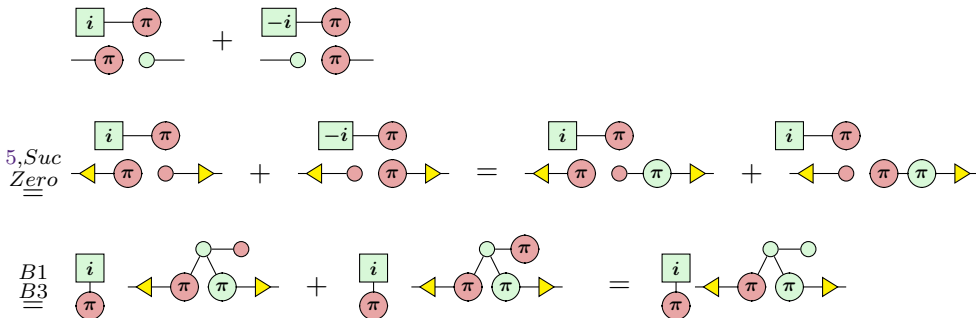
Proof.



□

Lemma 62. $\begin{matrix} \boxed{i} & \pi \\ \pi & \circ \end{matrix} + \begin{matrix} \boxed{-i} & \pi \\ \circ & \pi \end{matrix} = \begin{matrix} \frac{\pi}{2} & \pi & -\frac{\pi}{2} \end{matrix}$

Proof. We use the triangle to do the change of basis from $|+\rangle$ and $|1\rangle$ to $|0\rangle$ and $|1\rangle$.



The rest of the proof is identical to the proof of Lemma 59. □

Lemma 63.

Proof.

□

Lemma 64.

Proof.

□

Lemma 65.

Proof.

□

B Integration proofs

Lemma 21. Let k be a non-zero integer and M a diagram with no occurrence of θ . Then

$$\frac{1}{2\pi} \int_{-\pi}^{\pi} \left. \begin{array}{c} n \\ \vdots \\ k\theta \\ \vdots \\ k\theta \\ \vdots \\ m \end{array} \right\} M \left. \begin{array}{c} \vdots \\ -k\theta \\ \vdots \\ -k\theta \\ \vdots \\ l \end{array} \right\} d\theta = \sum_{\substack{\vec{x}, \vec{y} \in \{0,1\}^n \\ w(\vec{x})=w(\vec{y})}} \left. \begin{array}{c} x_1\pi \\ \vdots \\ x_n\pi \\ \vdots \\ m \end{array} \right\} M \left. \begin{array}{c} \vdots \\ y_1\pi \\ \vdots \\ y_n\pi \\ \vdots \\ l \end{array} \right\}$$

Proof. We have

$$\textcircled{k\theta} \text{---} \stackrel{(Z)}{=} \textcircled{\cdot} \text{---} + e^{ik\theta} \textcircled{\pi} \text{---} = \sum_{x \in \{0,1\}} e^{ik\theta x} \textcircled{x\pi} \text{---} \quad (4)$$

Thus, we can decompose our diagram as follows:

$$\begin{aligned} & \begin{array}{c} \textcircled{k\theta} \text{---} \\ \vdots \\ \textcircled{k\theta} \text{---} \\ \vdots \\ \text{---} \\ \vdots \\ \text{---} \end{array} \begin{array}{c} \vdots \\ \vdots \\ \vdots \\ \vdots \\ \vdots \\ \vdots \end{array} \begin{array}{c} \text{---} \\ \vdots \\ \text{---} \\ \vdots \\ \text{---} \\ \vdots \\ \text{---} \end{array} \stackrel{(4)}{=} \sum_{\vec{x} \in \{0,1\}^n} e^{ik\theta w(\vec{x})} \begin{array}{c} \textcircled{x_1\pi} \text{---} \\ \vdots \\ \textcircled{x_n\pi} \text{---} \\ \vdots \\ \text{---} \\ \vdots \\ \text{---} \end{array} \begin{array}{c} \vdots \\ \vdots \\ \vdots \\ \vdots \\ \vdots \\ \vdots \end{array} \begin{array}{c} \text{---} \\ \vdots \\ \text{---} \\ \vdots \\ \text{---} \\ \vdots \\ \text{---} \end{array} \\ & \stackrel{(4)}{=} \sum_{\vec{x}, \vec{y} \in \{0,1\}^n} e^{ik\theta(w(\vec{x})-w(\vec{y}))} \begin{array}{c} \textcircled{x_1\pi} \text{---} \\ \vdots \\ \textcircled{x_n\pi} \text{---} \\ \vdots \\ \text{---} \\ \vdots \\ \text{---} \end{array} \begin{array}{c} \text{---} \\ \vdots \\ \text{---} \\ \vdots \\ \text{---} \\ \vdots \\ \text{---} \end{array} \begin{array}{c} \text{---} \\ \vdots \\ \text{---} \\ \vdots \\ \text{---} \\ \vdots \\ \text{---} \end{array} \end{aligned} \quad (5)$$

Furthermore, for every integer $a \in \mathbb{Z}$, we have

$$\frac{1}{2\pi} \int_{-\pi}^{\pi} e^{ia\theta} d\theta = \begin{cases} 1 & \text{if } a = 0 \\ \frac{2 \sin(a\pi)}{a} = 0 & \text{if } a \neq 0 \end{cases} \quad (6)$$

Therefore, we can conclude

$$\begin{aligned} & \frac{1}{2\pi} \int_{-\pi}^{\pi} \begin{array}{c} \textcircled{k\theta} \text{---} \\ \vdots \\ \textcircled{k\theta} \text{---} \\ \vdots \\ \text{---} \\ \vdots \\ \text{---} \end{array} \begin{array}{c} \vdots \\ \vdots \\ \vdots \\ \vdots \\ \vdots \\ \vdots \end{array} \begin{array}{c} \text{---} \\ \vdots \\ \text{---} \\ \vdots \\ \text{---} \\ \vdots \\ \text{---} \end{array} d\theta \stackrel{(5)}{=} \sum_{\vec{x}, \vec{y} \in \{0,1\}^n} \left(\frac{1}{2\pi} \int_{-\pi}^{\pi} e^{ik\theta(w(\vec{x})-w(\vec{y}))} d\theta \right) \begin{array}{c} \text{---} \\ \vdots \\ \text{---} \\ \vdots \\ \text{---} \\ \vdots \\ \text{---} \end{array} \\ & \stackrel{(6)}{=} \sum_{\substack{\vec{x}, \vec{y} \in \{0,1\}^n \\ w(\vec{x})=w(\vec{y})}} \begin{array}{c} \text{---} \\ \vdots \\ \text{---} \\ \vdots \\ \text{---} \\ \vdots \\ \text{---} \end{array} \end{aligned}$$

□

Lemma 66. Σ_1 is symmetric:

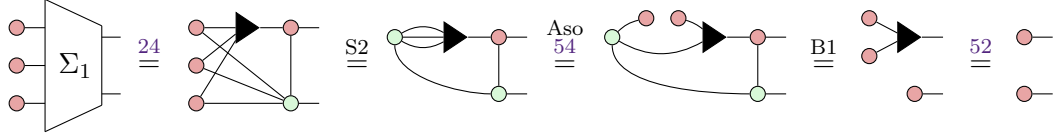
$$\begin{array}{c} \text{---} \\ \vdots \\ \text{---} \\ \vdots \\ \text{---} \end{array} \Sigma_1 \begin{array}{c} \text{---} \\ \vdots \\ \text{---} \\ \vdots \\ \text{---} \end{array} = \begin{array}{c} \text{---} \\ \vdots \\ \text{---} \\ \vdots \\ \text{---} \end{array} \Sigma_1 \begin{array}{c} \text{---} \\ \vdots \\ \text{---} \\ \vdots \\ \text{---} \end{array} = \begin{array}{c} \text{---} \\ \vdots \\ \text{---} \\ \vdots \\ \text{---} \end{array} \Sigma_1 \begin{array}{c} \text{---} \\ \vdots \\ \text{---} \\ \vdots \\ \text{---} \end{array} = \begin{array}{c} \text{---} \\ \vdots \\ \text{---} \\ \vdots \\ \text{---} \end{array} \Sigma_1 \begin{array}{c} \text{---} \\ \vdots \\ \text{---} \\ \vdots \\ \text{---} \end{array}$$

Proof. Immediately follows from the definition of Σ_1 and (Sym). □

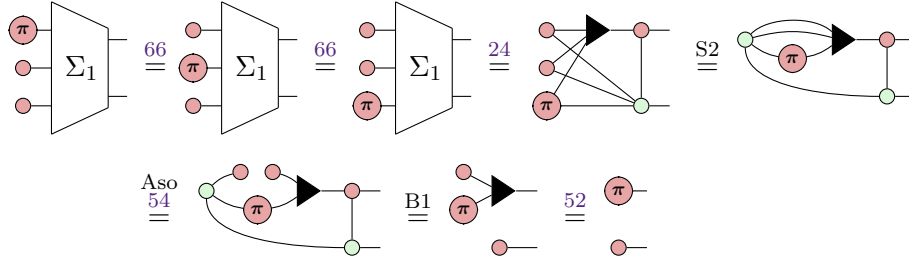
Lemma 25. Σ_n performs binary addition, i.e. for all $\vec{x}, \vec{y} \in \{0,1\}^n$ and $c \in \{0,1\}$, we have $\Sigma_n |c, \vec{x}, \vec{y}\rangle = |\vec{z}\rangle$ where $[\vec{z}] = [\vec{x}] + [\vec{y}] + c$.

Proof. The inductive construction follows the structure of a basic ripple-carry adder [35]. It suffices to verify that Σ_1 acts like a full-adder on computational basis states.

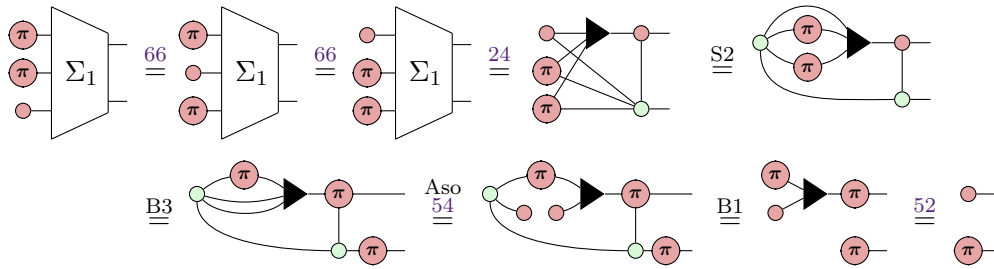
For the all-zero state, we have



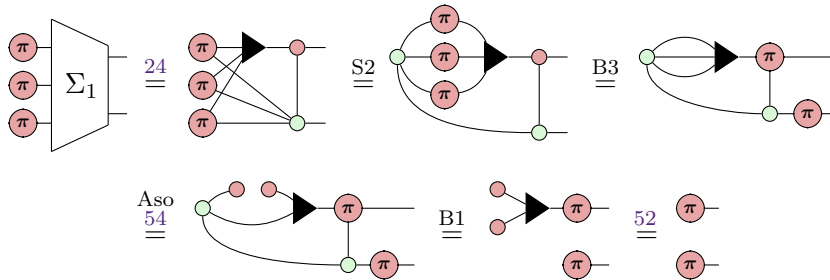
For states with one bit turned on, we have



For states with two bits turned on, we have



Finally, for the all-one state, we have

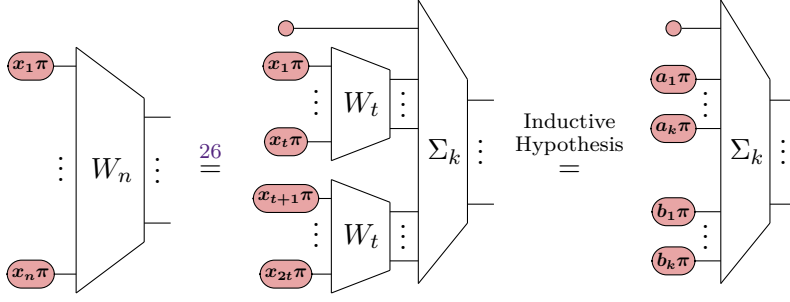


□

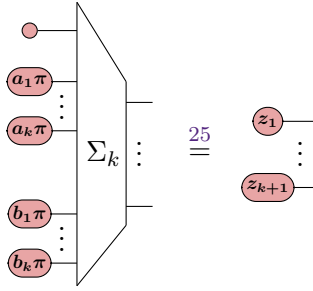
Lemma 28. W_n computes the binary Hamming weight, i.e. for all $\vec{x} \in \{0, 1\}^n$, we have $W_n |\vec{x}\rangle = |\vec{z}\rangle$ where $[\vec{z}] = w(\vec{x})$.

Proof. By induction on n . W_1 is trivially correct since the Hamming weight of a single bit is equal to its value. Now suppose that the lemma holds for all $l < n$. If n is even, i.e.

$n = 2t$ for some $t < n$, then



where $k = \lfloor \log(t) \rfloor + 1$, $[\vec{a}] = w(x_1, \dots, x_t)$, and $[\vec{b}] = w(x_{t+1}, \dots, x_{2t})$. Then



where $[\vec{z}] = [\vec{a}] + [\vec{b}] + 0 = w(x_1, \dots, x_t) + w(x_{t+1}, \dots, x_{2t}) = w(\vec{x})$ as required.

The case where n is odd follows similarly. □

Proposition 27. *The diagram size of W_n only grows linearly with increasing n .*

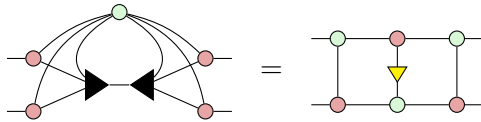
Proof. We denote the size of a ZX diagram D as $S(D)$. In the following, we only consider the size in big-O notation.

Clearly, we have $S(\Sigma_n) \in O(n)$. Following the definition of W_n , we thus have

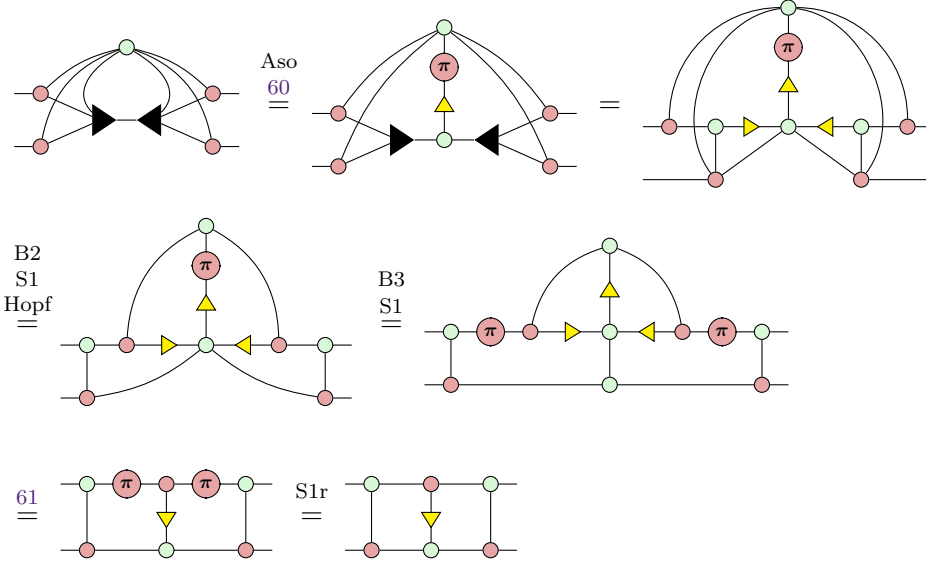
$$\begin{aligned} S(W_1) &= O(1), & S(W_n) &= 2S(W_{n/2}) + S(\Sigma_{\lfloor \log n \rfloor + 1}) && \text{for } n > 1 \\ & & &= 2S(W_{n/2}) + O(\lfloor \log n \rfloor + 1) \end{aligned}$$

The Master theorem [7] implies that this recurrence relation satisfies $S(W_n) \in O(n)$. □

Lemma 67.



Proof.



□

C Barren Plateau Analysis

Lemma 35. [52] Given $\langle H \rangle$ in the form of (2), we have $\mathbf{E} \left(\frac{\partial \langle H \rangle}{\partial \theta_j} \right) = 0$, for $j = 1, \dots, m$.

Proof. By integrating over the uniform distribution, we have

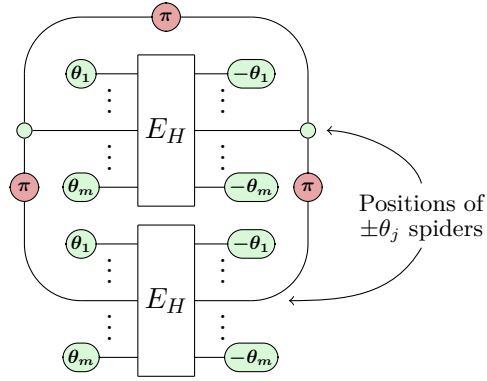
$$\mathbf{E} \left(\frac{\partial \langle H \rangle}{\partial \theta_j} \right) = \frac{1}{(2\pi)^m} \int_{-\pi}^{\pi} \dots \int_{-\pi}^{\pi} \frac{\partial \langle H \rangle}{\partial \theta_j} d\theta_1 \dots d\theta_m.$$

We prove the theorem by showing that $\frac{1}{2\pi} \int_{-\pi}^{\pi} \frac{\partial \langle H \rangle}{\partial \theta_j} d\theta_j = 0$.

$$\begin{aligned} \frac{\partial \langle H \rangle}{\partial \theta_j} &\stackrel{18}{=} \text{Diagram 1} \\ \frac{1}{2\pi} \int_{-\pi}^{\pi} \frac{\partial \langle H \rangle}{\partial \theta_j} d\theta_j &\stackrel{32}{=} \text{Diagram 2} \\ &\stackrel{63}{=} \text{Diagram 3} = 0 \end{aligned}$$

Since the unconnected pink π spider is equal to the zero scalar, the entire diagram evaluates to zero. □

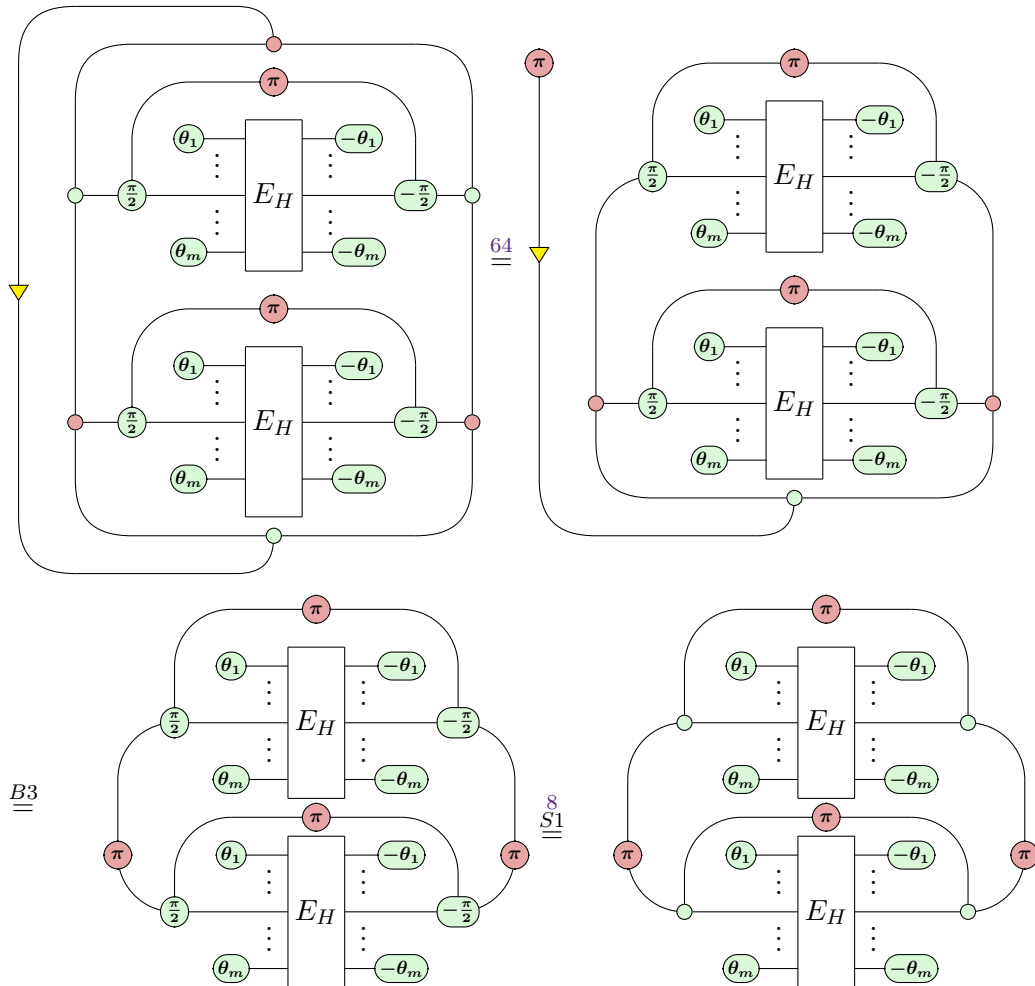
Lemma 36. [52] Given $\langle H \rangle$ in the form of (2), we have

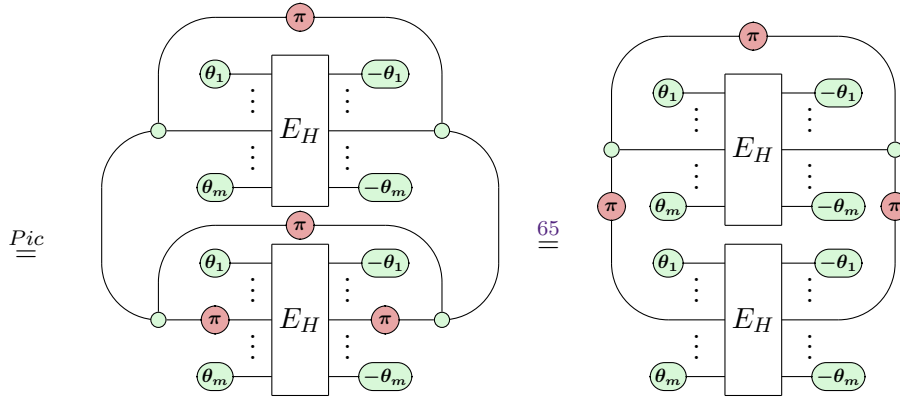
$$\frac{1}{2\pi} \int_{-\pi}^{\pi} \left(\frac{\partial \langle H \rangle}{\partial \theta_j} \right)^2 d\theta_j =$$


where the cycle connects the legs of E_H that correspond to the positions of the $\pm\theta_j$ spiders in (2).

Proof. By Example 33,

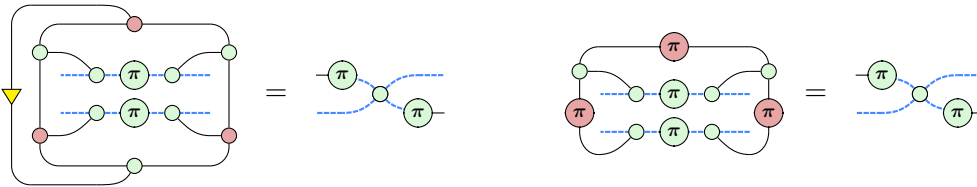
$$\frac{1}{2\pi} \int_{-\pi}^{\pi} \left(\frac{\partial \langle H \rangle}{\partial \theta_j} \right)^2 d\theta_j =$$



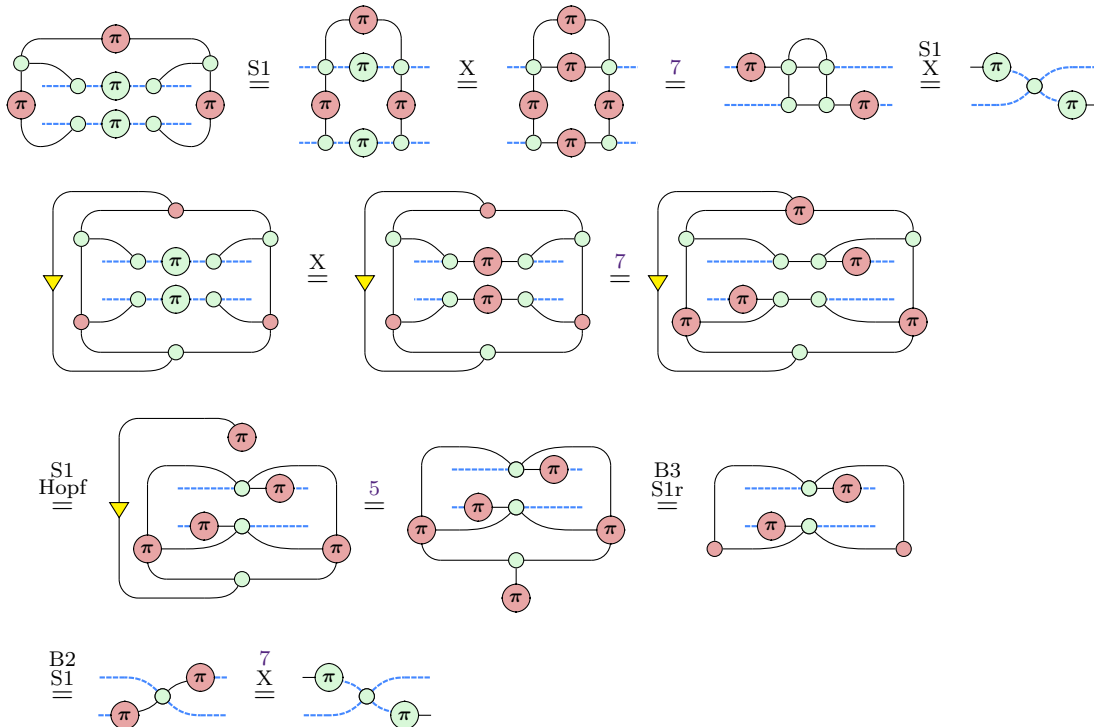


□

Lemma 40. *The cycles in diagram (3) can be broken up as follows.*

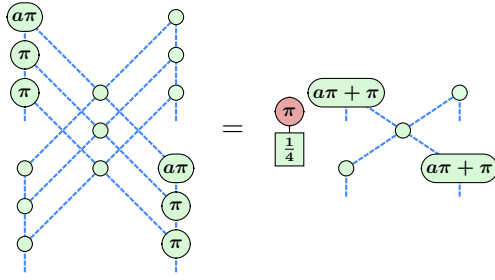


Proof.

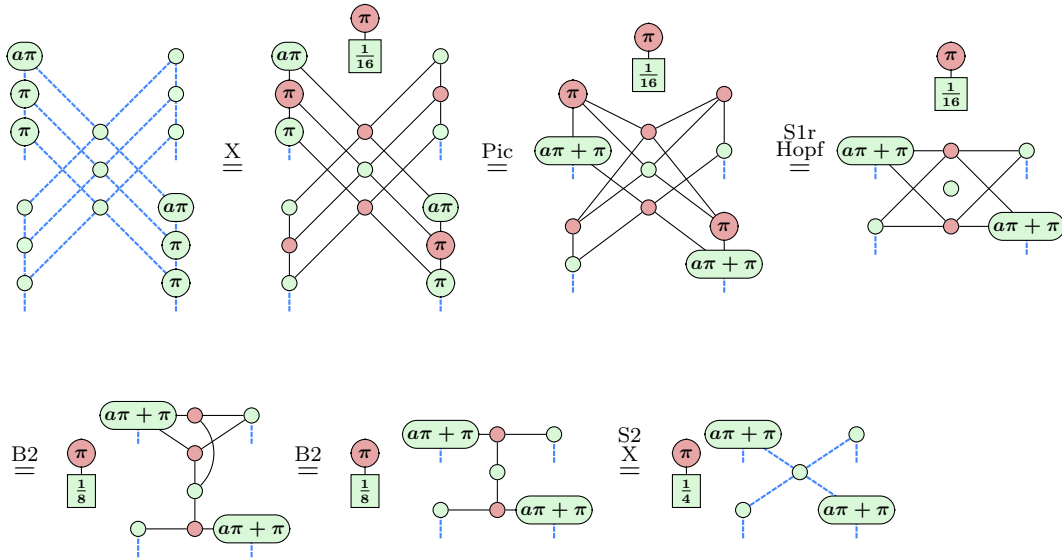


□

Lemma 68. For all $a \in \{0, 1\}$, we have



Proof.



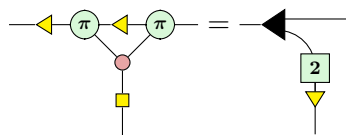
□

D Comparison with Jeandel et al.

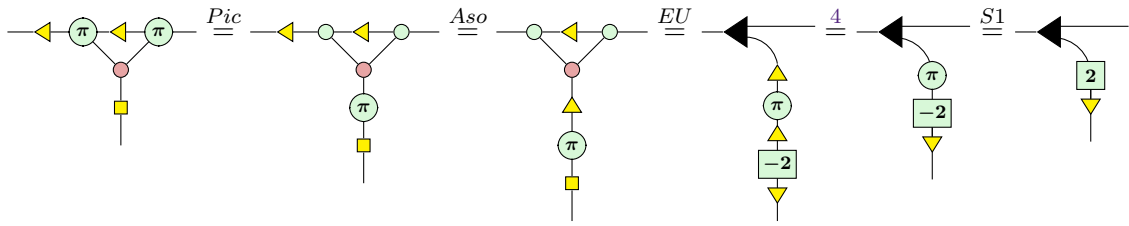
Jeandel, Perdrix, and Veshchezerova present an alternate method to represent derivatives with the ZX-calculus [24]. We want to show that the two papers arrive at similar results through very different techniques, and that some results in [24] can be more compactly represented by explicitly using the W spider. The nodes used in [24] are similar to ours: the circle green nodes, the Hadamard node and the red nodes are exactly the same, but we additionally have pink nodes which are different to the red nodes up to a variational scalar, and have green box nodes which have the circle green nodes as special cases while can be turned into circle green nodes with the help of the yellow triangle node [23]. Also note that their black triangle corresponds to our yellow triangle and our black triangle corresponds to the W spider.

First, we show that the triangular-shaped diagram that features in their differentiation result can be represented compactly using the W spider:

Lemma 69.

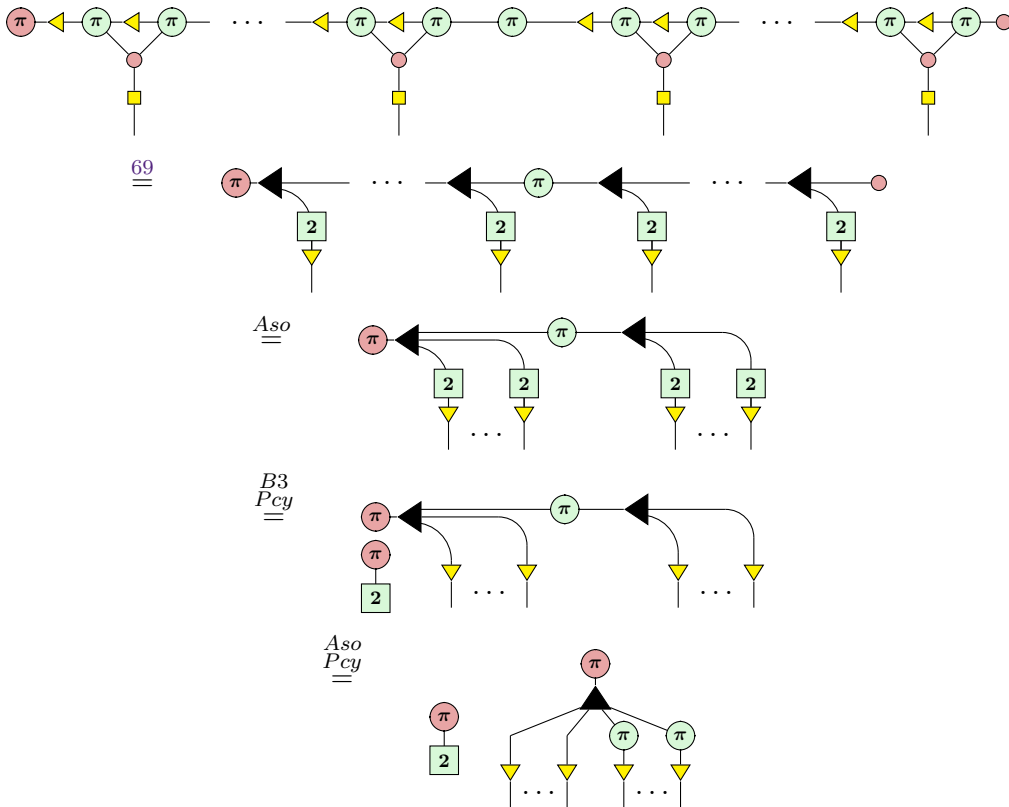


Proof.



□

Remark 70. The differentiation of “linear” ZX diagrams result obtained by [24] is equivalent to our lemma 17.



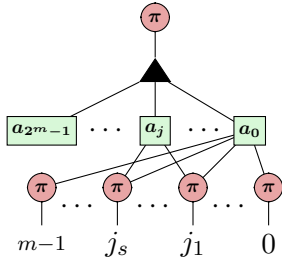
Although the end results are equivalent, we emphasise that their result is obtained through their theory of summing controlled diagrams, whilst our result is obtained through our arbitrary differentiation result.

Remark 71. The general differentiation result in [24] requires an inductive conversion to controlled diagrams, and is obtained through combining diagrammatic addition and the Leibniz product rule. Because of this, the resulting diagram will not resemble the original diagram.

In comparison, our Theorem 14 does not affect the topology of the original diagram and can be calculated almost instantly.

Remark 72. Both the general results on addition of diagrams and on differentiation of diagrams shown in [24] are based on induction on generators. If such induction methods

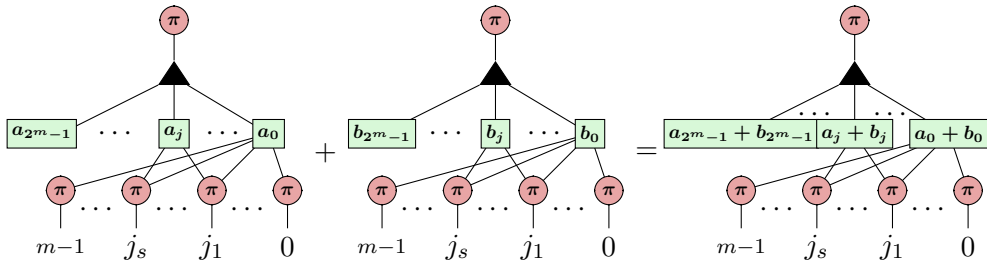
are allowed, then there is an alternative way to generally add two ZX diagrams or differentiate a ZX diagram: first rewrite inductively the diagrams into the compressed normal form shown in [48] as follows



which corresponding to the vector

$$\begin{pmatrix} a_0 \\ a_1 \\ \vdots \\ a_{2^m-2} \\ a_{2^m-1} \end{pmatrix},$$

then the sum of two diagrams can be obtained by adding up the corresponding parameters in the two diagrams:



and the differentiation can be obtained element-wisely:

